Materials Advances

ROYAL SOCIETY OF CHEMISTRY

PAPER

View Article Online
View Journal | View Issue

Check for updates

Cite this: *Mater. Adv.*, 2024, 5, 4504

Selective induction of apoptotic cell death in lung carcinoma cells by curcumin-loaded PEGylated lipid nanoparticles with minimal normal tissue toxicity: *in vitro* and *in vivo* toxicity evaluation by oral delivery†

Bijaideep Dutta,[ab] Sourav Kumar Das,[bc] Mayur Temgire,[de] Jayesh Bellare,[e] K. C. Barick,*[ab] Amit Kumar[bc] and P. A. Hassan*[ab]

Received 16th January 2024,
Accepted 2nd April 2024

DOI: 10.1039/d4ma00050a

rsc.li/materials-advances

Insufficient drug concentration, systemic toxicity in associated organs and meaningful penetration to the site of action remain major challenges in augmenting the therapeutic efficacy against heterogeneous diseases such as lung cancer, which have become a major burden to society. In this case, oral delivery of smart nanoparticles can offer better patient compliance compared to the intravenous administration routes. Herein, we demonstrate a strategy to produce curcumin-loaded sub-micron sized PEGylated lipid particles (CSLNs) with a controlled size and narrow polydispersity to expand the chemotherapeutic treatment of lung cancer, which could inhibit the migration and invasion of cancer cells. PEGylation improved the stability and bioavailability of curcumin. These CSLNs (10, 20 and 40 μM) were found to induce preferential toxicity in a non-small cell lung cancer cell line (A549) by altering its morphology and induction of apoptosis in a concentration and time-dependent manner compared to normal lung epithelial cells (WI26). The high cytotoxicity of CSLNs was attributed to their higher internalization in the cancer cells (~2.0–4.5 fold) compared to the normal lung cells. Confocal microscopy revealed the significantly higher accumulation of curcumin (2–4 fold) in the nucleus of the lung cancer cells. Flow cytometry analysis further revealed that the percentage of cells in the sub-G1 phase was significantly higher when treated with CSLNs compared to the bare CUR-treated A549 cells. The *in vivo* sub-acute toxicity studies indicated that the CSLNs were free from any adverse side effects upon oral administration up to a dose of 200 mg kg^{-1} day^{-1} for 28 days. The histopathological analysis and haematological parameters indicated that there was no significant alteration in the cellular mechanism or metabolic activity of the SLN-treated cells. Thus, this rationally designed oral delivery vehicle provides a promising approach for lung cancer therapy with minimum systemic toxicity.

1. Introduction

The predominant sub-type of non-small cell lung cancer (NSCLC) is responsible for the most cancer-related deaths worldwide, accounting for around 11.4% of total cancer and 18% of total cancer deaths in men.[1–3] In general, lung cancer originates inside the bronchial epithelium, which receives approximately less than 1% cardiac blood output mostly by bronchial arteries.[4,5] Regrettably, most cases of lung cancer are diagnosed at a very late stage, *i.e.* only after it enters the metastatic stage. This metastasis to remote organs such as the liver, bone, and nervous system is the leading reason behind the poor survival rate in lung cancer patients (5 year survival rate of only 10%).[6,7] Most of the small chemotherapeutic molecules used for lung cancer treatment are highly water insoluble (highly hydrophobic in nature). Thus, the insignificant bioavailability of drugs also is another reason for concern. Moreover, the blood flow into the bronchial epithelium is very low, and thus the typical concentration of the anti-cancer drug

[a] *Chemistry Division, Bhabha Atomic Research Centre, Trombay, Mumbai 400085, India. E-mail: kcbarick@barc.gov.in, hassan@barc.gov.in; Fax: +91 22 2550 5099; Tel: +91 22 2559 0284*
[b] *Homi Bhabha National Institute, Anushaktinagar, Mumbai 400094, India*
[c] *Radiation Biology and Health Science Division, Bhabha Atomic Research Centre, Trombay, Mumbai 400085, India*
[d] *Advanced Centre for Treatment, Research and Education in Cancer (ACTREC), Navi Mumbai 410210, India*
[e] *Indian Institute of Technology, Bombay, Powai, Mumbai 400076, India*
† Electronic supplementary information (ESI) available. See DOI: https://doi.org/10.1039/d4ma00050a

required for exhibiting tumor cell killing efficacy in the lung cancer microenvironment remains difficult to achieve.[8,9]

Thus, the general treatment modalities such as systemic chemotherapy *via* intravenous administration do not have the capability for tackling lung carcinoma due to their suboptimal drug concentrations at the site of action and rather considerable distribution of the chemotherapeutic agent in various non-targeted organs. This low drug concentration at the desired site necessitates an elevated dosing rate of the chemotherapeutic agent, which leads to undesirable toxicity and consequent adverse effects to organs such as the hair, liver, spleen and skin.[10] Also, the very high tumor interstitial fluid pressure (TIFP) due to perivascular fibrosis and abnormal lymphatic drainage is another key reason for the poor therapeutic outcome of conventional chemotherapy. Furthermore, although i.v. delivery takes a fully bioavailable, accurate dose of the drug to the body immediately, it has some major side effects such as neurotoxicity, nephrotoxicity, myelosuppression, cardiotoxicity, ototoxicity, nausea, vomiting, diarrhea, and hair loss.[11,12] In many cases, some injectable anticancer drugs are formulated using particular toxic excipients such as cremophore in the case of paclitaxel.[13] Furthermore, i.v. chemotherapy is highly painful, causing bleeding and venous thrombosis, and hence the quality of life of the patient is compromised heavily.[14] Accordingly, surgical removal becomes the only option to treat non-metastatic lung cancer, which is further limited by the site of interest and the overall health status of the patient. Thus, in comparison to the parenteral route, the oral chemotherapy route is the preferred regimen for the treatment of chronic diseases such as cancer because of its benefits such as patient compliance and ease of administration, which can realize a sustained concentration of the drug in the plasma and limit an excessive concentration above the tolerable amount.[15] Nevertheless, most anticancer drugs are not orally bioavailable due to the special physiological properties of the GI tract, and hence their instability.

Therefore, the precise design of nanocarriers is necessary for improving the aqueous dispersibility and stability of drugs to greatly enhance lung cancer diagnosis and therapy. Nanoparticulate systems provide additional advantages for the delivery of anticancer drugs over the conventional chemotherapeutic modules using both passive and active targeting pathways. In the case of passive targeting, the nanoparticle-mediated delivery system enables the augmented accumulation of the drug-loaded formulation at the cancer sites due to the leaky vasculature of the cancer tissue as a result of its enhanced permeability, which has been documented *in vivo*.[16–18]

The natural polyphenol curcumin is basically an α,β-unsaturated β-diketone, which exists in equilibrium with its enol tautomer with wide range of pharmacological effects. In acidic or neutral medium and in cell membranes the keto form predominates, whereas the enol form is dominant in alkaline medium by having a heptadienone chain-like structure. The keto–enol tautomerism equilibrium of the heptadienone moiety of curcumin determines its physicochemical properties. *In vitro* and *in vivo* studies have shown the efficacy of curcumin in inhibiting lung carcinogenesis, tumor cell proliferation and metastasis.[19–22] However, despite its promising therapeutic effects, the commercial application of curcumin for cancer therapy has not yet realised because upon oral or intravenous/intraperitoneal administration, it is rapidly eliminated from the body due to its poor water solubility (around 400 ng mL^{-1} at pH 7.4), chemical instability, and consequent degradation in the gastrointestinal tract under physiological conditions followed by non-bioavailability. A series of pH-dependent studies has shown that curcumin undergoes rapid decomposition under neutral-basic condition with the formation of *trans*-6-(4-hydroxy-3-methoxyphenyl)-2,4-dioxo-5-hexenal as the main degradation product.[23] Upon administration, curcumin undergoes metabolism to form curcumin glucuronide and curcumin sulfate at first *via* *o*-conjugation, followed by bio-reduction to produce tetrahydrocurcumin, hexahydrocurcumin, octahydrocurcumin, and hexahydrocurcuminol in rats, mice and humans *in vivo*.[24] Subsequently, the reduced curcumin undergoes glucuronidation and is converted into curcumin glucuronide, dihydro-curcumin-glucuronide, tetrahydrocurcumin-glucuronide, and curcumin sulfate. Therefore, it is necessary to develop highly efficient stable nanoformulations of curcumin that can protect the curcumin moiety under physiological conditions after oral administration with enhanced concentration.[25,26] Among the various nanoformulations, the use of solid lipid nanoparticles appears to be a promising strategy to improve the drug loading and photostability of curcumin.[27] The solid structure of lipids permits a high loading of the active ingredient and effectively protects the drug from external factors such as light and pH. Taratula *et al.* demonstrated the efficacy of lipid-based nanocarriers for the effective and selective deposition of doxorubicin and si-RNA in lung tumor cells by minimizing their deposition in healthy lung tissues.[28] Further, surface modification using polyethylene glycol (PEG) has also been found to be a great strategy to reduce opsonization, minimize the clearance by the mononuclear phagocyte system (MPS) and non-specific protein adsorption.[29,30]

Thus, in the present study, we report a novel method for developing sub-micron-sized PEGylated curcumin-loaded solid lipid nanoparticles (CSLNs) with a narrow polydispersity and long-term colloidal stability. These CSLNs (10, 20 and 40 μM) were found to induce preferential toxicity in a non-small cell lung cancer cell line (A549) by altering its morphology and induction of apoptosis in a concentration-dependent manner compared to normal lung epithelial cells. Furthermore, to evaluate the sub-acute toxicity limit of the developed oral-based nanoformulation, *in vivo* sub-acute toxicity studies were performed. These studies indicated that this nanoformulation is completely free from any adverse side effects upon oral administration up to a dose of 200 mg kg^{-1} day^{-1} for 28 days. The histopathological analysis and haematological parameters indicated that there was no significant alteration in the cellular mechanism or metabolic activity of the CSLN-treated cells.

2. Experimental

2.1. Preparation of curcumin-loaded solid lipid nanoparticles (CSLNs)

The hydrophobic drug curcumin-loaded nanoparticles (CSLNs) were prepared *via* the emulsification and low-temperature solidification method.[31] Briefly, curcumin (0.145 g), lauric acid (0.22 g) and lecithin (0.175 g) were added to 10 mL of chloroform. Subsequently, this mixture was dissolved by ultrasonication to prepare the organic phase. The obtained organic phase was added to an aqueous phase containing 0.275 g of P188 dissolved in 25 mL of distilled water. The mixture was stirred at 1000 rpm at 70 °C for approximately 90 min. The organic solvent was removed to obtain a very viscous system. The highly viscous system was placed in an ice-cold environment at 0–2 °C and added to 10 mL cold water followed by stirring at 1200 rpm for 1 h. Subsequently, the resultant suspension was centrifuged at 12 000 rpm to remove the supernatant. Finally, the collected precipitate was resuspended in ultrapure water and lyophilized in a table top lyophilizer. The dried powder was kept refrigerated for further use. The bare SLNs were prepared *via* the same procedure without the addition of curcumin.

2.2. Solubility of curcumin in CSLNs

To determine the solubility of the curcumin in CSLNs, CSLNs were centrifuged at 12 000 rpm for 60 min to remove any free curcumin, then the pellet was redispersed and aliquots were collected for UV spectrophotometry analysis with the absorption maximum at 422 nm.

2.3. Structural morphology determination

Dynamic light scattering (DLS) measurement was performed using a Malvern 4800 Autosizer employing a 7132 digital correlator for the determination of hydrodynamic diameter using a 632.8 nm He–Ne laser with a power of 15 mW. The zeta potential was estimated at 25 °C based on electrophoretic mobility with a Malvern Zeta-Sizer Nano ZS (Malvern Instruments, Southborough, UK). The cryo-TEM sample was prepared in a thin layer of vitrified sample on the Cu-grid. A small drop of sample was cast on the lacey-carbon coated Cu-grid. The excess liquid was bloated using filter paper and a Vitrobot plunging device. A thin layer of vitrified sample was formed on the sample Cu-grid. The sample Cu-grid was bloated and initially plunged in liquified ethane, and later transferred to liquid nitrogen to prevent the crystallization of the sample and avoid the loss of its inherent microstructures on the Cu-grid. The formation of crystalline ice would have degraded the quality of the images. Then, the sample grid was further transferred to a pre-cooled cryo-holder at −170 °C on the cryogenic station. Later, the cryo-holder was inserted in the cryo-TEM and it was allowed to equilibrate and attain a temperature of −170 °C for 15–20 min. The samples were observed by maintaining the cold chain throughout the process of cryo-EM sample preparation. The X-ray diffraction (XRD) analysis was performed on a Phillips PW1729 diffractometer with Cu Kα radiation (λ = 1.5405 Å) at an operating voltage of 40 kV and current of 40 mA. The scan rate was kept fixed at 2° per minute. The samples were finely grinded using a mortar pestle and placed on glass slide. Then, the slide was mounted on a goniometer for data collection. The FTIR spectra were recorded in the range 4000–400 cm^{-1} on an FTIR spectrometer (Bomen Hartmann and Braun, MB series) using KBr pellets and resolution of 4 cm^{-1}. Solid powder samples (~2–4 mg) were mixed with KBr (~200 mg) to prepare the pellets. The pellets were prepared by putting the KBr-sample mixture in press dies (10 mm diameter) inside a KBr press machine and pressure was applied 5 kg cm^{-2} for 2–3 min to produce solid pellets. Preliminary spectrum treatment involved 10-point smoothing and baseline correction between the first and last points.

2.4. Encapsulation efficiency (EE) and loading capacity (LC) of CSLNs

The amount of curcumin loaded in CSLNs was determined as follows: 1.4 mL of methanol was added to 2.8 mg of CSLNs, and the mixture was stirred at 37 °C for 90 min. The resulting mixture was centrifuged to separate the undissolved components. The supernatant contained the drug curcumin extracted from CSLNs. This curcumin solubilized in methanol was analysed using a UV spectrophotometer at 422 nm. The percent LC was calculated using eqn (1), as follows:

$$\%\,\mathrm{LC} = \frac{\text{Total quantity of drug in SLNs}}{\text{Total quantity of drug and excipients in SLNs}} \times 100 \quad (1)$$

The encapsulation efficiency was calculated as follows: 1 mL of the initially prepared CSLNs (stock sol.) was completely disrupted with addition of methanol by vortexing the solution, which contained the total curcumin concentration in the solution. Then the UV spectrum was recorded. After that, 1 mL of stock solution was taken and centrifuged at 12 000 rpm for 60 min. The supernatant containing the unencapsulated curcumin was collected and its UV spectrum was recorded.[32]

$$\%\,\mathrm{EE} = \frac{\text{Total Curcumin taken} - \text{Curcumin in supernatatnt (unecapsulated)}}{\text{Total curcumin}} \times 100 \quad (2)$$

2.5. *In vitro* release

A known amount of CSLN powder was dissolved in the buffer medium (2 mL) with different pH to mimic the intracellular condition in cancer tissue (pH 7.4, 6.5 and 5) and loaded in a dialysis bag (MWCO 10 kDa), which was placed in 100 mL of receptor medium (kept constant at 37 °C ± 0.5 °C and stirred at 100 rpm). The receptor medium had 0.1% Tween-80 for facilitating the release of curcumin in PBS (pH 7.4) (sink). A known amount of aliquot was taken from the sink and filled with PBS

of the same composition to maintain the volume. The content of curcumin in the released medium was determined at regular intervals using a UV spectrophotometer and calculated according to the calibration curve. The samples were protected from light throughout the procedure.[33]

2.6. Chemical stability

The chemical stability of CSLNs was assessed and compared with free curcumin in both PBS and DMEM medium with a final concentration of 20 μg mL^{-1} in 5 mL dispersion. The samples were incubated at 37 °C for 0, 15 min, 30 min, 60 min and 6 h. At each interval, 150 μL sample was taken and dissolved in 550 μL of methanol. Subsequently, the samples were vortexed for 1 min and centrifuged at 12 000 rpm for 5 min and stored on ice prior to spectral analysis using a plate reader.[34]

2.7. Storage stability of CSLNs

CSLNs were stored at 4 °C for 2 months in 50 mL Falcon tubes wrapped in Al-foil in the dark. Then, the variation in the encapsulation efficiency, particle size and zeta potential was determined at predetermined intervals (1, 7, 14, 30, and 60 days).

2.8. *In vitro* study

2.8.1. Cell culture. Human lung adenocarcinoma cells (A549) and normal human lung epithelial cells (WI26 VA4, ECACC 89101301) were procured from the European Collection of Authenticated Cell Cultures (ECACC) and cultured in Dulbecco's modified Eagle's medium (DMEM) supplemented with 10% fetal calf serum (FCS), 2 mM glutamine, and penicillin–streptomycin (10 000 units per mL). Cells were seeded at the desired cell density in suitable culture plates in triplicate for control/treatment groups and placed in an incubator at 37 °C at 5% CO_2. After ~24 h, the medium was replaced with fresh medium with or without different concentrations of CSLN or CUR (10, 20 and 40 μM). The cells were treated with bare NP (SLN, 100 μg mL^{-1}) as the control treatment.

2.8.2. Phase contrast microscopy. To study the morphological changes, bright-field microscopy of the control and treated human adenocarcinoma cells (A549) as well as normal human lung epithelial cells (WI26) was performed after 24 h of various indicated treatments. Multiple images (8–10) per treatment group were taken at 20× magnification. The curcumin control (10–40 μM) was taken to compare the morphological alterations induced by CSLN.

2.8.3. MTT assay and cell count. To study the cytotoxic effect of CSLN treatment, the MTT (3-[4,5-dimethylthiazol-2-yl]-2,5-diphenyltetrazolium bromide) assay was performed as described previously.[35] Briefly, a specific number of cells (~3000 cells per well) was seeded in cell culture medium in a 96-well plate. After overnight attachment, the medium was replaced with CUR or CSLN (0, 10, 20 and 40 μM) having an equivalent concentration of curcumin as well as bare NPs (100 μg mL^{-1}) in the cell culture medium for 24–48 h. At the end of incubation, MTT solution (0.5 mg mL^{-1}) was added to each well for 3 h at 37 °C. MTT formazan crystals were dissolved in dimethyl sulfoxide (DMSO). The absorbance of each well was measured at 550 nm using a microplate reader (Infinite-200Pro, Tecan, Switzerland). Microwells (in quadruplicate) with medium only (without cells) were also kept as a blank control to check the effect of CUR on the reduction of MTT. The mean absorbance intensity was derived from five independent treatment/control groups. To further assess the effect of CSLNs on cell proliferation, a cell count analysis was performed. Briefly, a specific number of cells (5×10^5 cells per well for A549 or 2×10^5 cells per well for WI26) was seeded in cell culture medium in 6-well plates. After overnight attachment, the medium was replaced with CUR- or CSLN-containing medium having equivalent drug concentrations (0, 10, 20 and 40 μM) or bare NP (*i.e.* SLN, 100 μg mL^{-1}) to the cell culture medium for 24 h. Percentage cell proliferation was calculated as % proliferation = mean of absorbance of CUR- or CSLN-treated wells/absorbance mean of control wells × 100. Results were expressed as mean ± standard deviation (SD) of three independent experiments. Cell count was determined after 24 h of different treatments using an automatic cell counter (Denovix). Cell count experiments were performed in triplicate for each treatment group.

2.8.4. Immuno-fluorescence. A specific number of A549 and WI26 cells (~3000 cells per well) was seeded on cover slips (placed in a 6-well plate) for overnight attachment. For treatment, cells were incubated with pure CUR (0, 10, 20 and 40 μM) or CSLN having equivalent drug concentrations or bare NP (SLN, 100 μg mL^{-1}) in the cell culture medium for 24 h. The cells were processed for immune fluorescence analysis by following the method described previously. At the end of treatment, the cells were washed with PBS three times and fixed in 4% paraformaldehyde for 20 min at room temperature. After fixing, the cells were washed with PBS and mounted on a glass slide using cell mounting medium containing DAPI (Fluoroshield, Sigma) for nuclear staining. Subsequently, these cells were imaged using a confocal microscope (Olympus FV 3000, Japan) at the excitation wavelength (λ_{ex}) of 405 nm and 488 nm for DAPI and CUR, respectively.

To quantify the fluorescence of curcumin in the nucleus of the A549 and WI26 cells, the Image J software (NIH) was utilized. Briefly, the region of interest (ROI) in the merged images was selected by taking the margin of nucleus from the DAPI-only images as a reference. The fluorescence intensity was measured using the analysis tool in Image J. About 80–100 cells were analysed from 10–15 randomly selected images per treatment in triplicate. The relative fold change compared to the control was plotted for the various treatment groups.

2.8.5. Cell cycle analysis. To quantify the apoptotic mode of cell death by CSLN, FACS analysis was performed on propidium iodide (PI)-stained cells after various treatments. The cells (1×10^6) were plated in 60-mm culture dishes for overnight attachment, and then treated with CSLN or CUR for 24 h. At the end of treatment, the cells together with the supernatant were collected by trypsinization and washed twice with PBS and processed for PI staining as described previously (Manjoor

et al., 2014). The cells were fixed in ice-cold 70% ethanol for 1 h and stained with PI (50 μg mL^{-1}) for cell-cycle analysis. Events (20 000 per sample) were acquired with an FACScan flow cytometer (Cyflow space, Partec, Germany) and analyzed using the Cyflogic software to quantify the cells in sub-G1 peak.

2.8.6 RBC isolation and hemolysis assay. A hemolysis assay was used to investigate the compatibility of red blood cells with CSLN under physiological buffer condition. Human blood samples were obtained from healthy donors in the Pathology Lab, Medical Division, BARC, Mumbai with the approval of the Institutional Medical Ethics Committee. Blood samples were collected in heparinized tubes by vein puncture. RBC isolation was done at 4 °C following the standard protocol, as described earlier.[36] Briefly, blood (2 mL) was washed with 8 mL of HEPES-buffered saline (HBS) by centrifugation (1000*g*, 10 min) at 4 °C. After removing the supernatant, the cell pellet was resuspended in HBS (2 mL) and the cell concentration was determined by hemocytometry. The cell count, *i.e.* 5×10^7 cells per mL, was used for the hemolysis experiments. To determine the biocompatibility of CSLN, RBC suspensions were incubated with an increasing concentration of CSLN (1–50 μM, 2 h) followed by the quantification of hemolysis. At the end of incubation, the samples were centrifuged at 5000*g* for 10 min at room temperature and an image of the representative tubes was taken. Hemolysis was measured at 540 nm using a spectrophotometer (Jasco-V550, Japan). The percentage hemolysis was calculated using the formula: hemolysis (%) = [Abs. in the supernatant of treated samples/Abs. in the supernatant of 100% lysed samples] × 100. The untreated erythrocyte suspensions were completely lysed by adding 20 times the volume of distilled water.

2.8.7. Statistical analysis. Results are expressed as mean ± standard deviation. The Student's *t*-test was used to test the significant difference between the control and treated samples. Values of $p < 0.05$ were considered statistically significant.

2.9. *In vivo* toxicity study

2.9.1. Ethics statement and animals used. *In vivo* studies were performed according to the Institutional Animal Ethics Committee (IAEC) guidelines. A total of 15 healthy female Swiss mice (12 weeks old; weight 20–25 g) was included in this study. The mice were divided into three groups (two treatment groups, *i.e.*, bare SLN and CSLNs, and one control group) and used for the oral toxicity investigations. They were kept in the Experimental Animal Facility of the Bhabha Atomic Research Centre, Trombay under controlled environmental conditions of adequate ventilation, about 23 ± 2 °C temperature, 60 ± 10% relative humidity, and 12 h dark and 12 h light cycle, with food and water *ad libitum*.[37] All animals were randomly assigned to cages for at least 7 days before the start of the experimentation. All cages were monitored daily and bedding material was changed thrice a week.

2.9.2. Sub-acute oral toxicity study. The required quantity of blank SLN and CSLNs was weighed according to the dose mentioned (200 mg kg^{-1} body weight) and suspended in nano pure water to get the desired concentration. The formulations were prepared shortly before dosing from the lyophilized powder form. The homogeneity of the formulation was conserved by continuous stirring on a magnetic stirrer during dosing. Using a gavaging needle, the formulation was administered by oral gavage to each mouse once daily, for a period of 28 d. The dosage volume for each mouse was adjusted according to its body weight on the day of dosing by maintaining the dosage volume of 10 mL kg^{-1}.[38] Animals were observed for morbidity and mortality twice daily. The body weights for all groups were measured prior to gavage on day 1 and weekly until and on the day of sacrifice.[39]

2.9.3. Sample collection and histopathological study. On day 28, all animals were weighed and sacrificed (by CO_2 asphyxiation). They were euthanized by cardiac puncture and their carcasses disposed. At the completion of the experimental period, all animals were fasted for 12 h prior to sacrifice. The obtained blood samples were immediately divided into two portions, one for hematological analysis (stored in an EDTA tube) and one for serum biochemistry. For histological examination, internal organs including the liver, lung, kidney, heart, and spleen were collected and immediately fixed in 10% buffered formalin. Further, the samples were fixed in paraformaldehyde for 24 h, followed by incubation in a gradient concentration of sucrose solution. The tissues were processed using an Automatic Tissue Processor and embedded with paraffin. The paraffin-embedded tissues were cut using a Microm HM 315 microtome and stained with haematoxylin and eosin (H&E). The slides were observed under a light microscope.[40]

2.9.4. Haematological and biochemical parameters. The estimated haematology parameters included haemoglobin (Hb), erythrocyte count (RBC), total leukocyte count (WBC), mean corpuscular volume (MCV), mean corpuscular haemoglobin (MCH), mean corpuscular haemoglobin concentration (MCHC) and platelet counts.[41] Blood smears were prepared with Leishman's stain and differential WBC or leucocyte count (DLC) was carried out by standard microscopy and counting 100 cells such as neutrophils (N), lymphocytes (L), eosinophils (E), monocytes (M) and basophils (B). The serum biochemistry parameters such as total serum bilirubin (mg dL^{-1}), direct serum bilirubin (mg dL^{-1}), serum total proteins (g dL^{-1}), serum total albumin (g dL^{-1}), serum total globulin (g dL^{-1}), albumin, alanine aminotransferase (ALT, IU L^{-1}), aspartate aminotransferase (AST, IU L^{-1}), alkaline phosphatase (IU L^{-1}), blood urea nitrogen (mg dL^{-1}), random blood sugar (mg dL^{-1}), total cholesterol (mg dL^{-1}), triglycerides (mg dL^{-1}), creatinine (mg dL^{-1}), Cl, Na and K (mEq L^{-1}) were also measured. All blood samples were analyzed, with the results reported as mean ± SD.

3. Results and discussion

3.1. Solubility and physiochemical characterization of CSLNs

Curcumin is a hydrophobic molecule, and hence has poor solubility in aqueous medium. In this case, the aqueous dispersibility of curcumin could be improved by incorporating

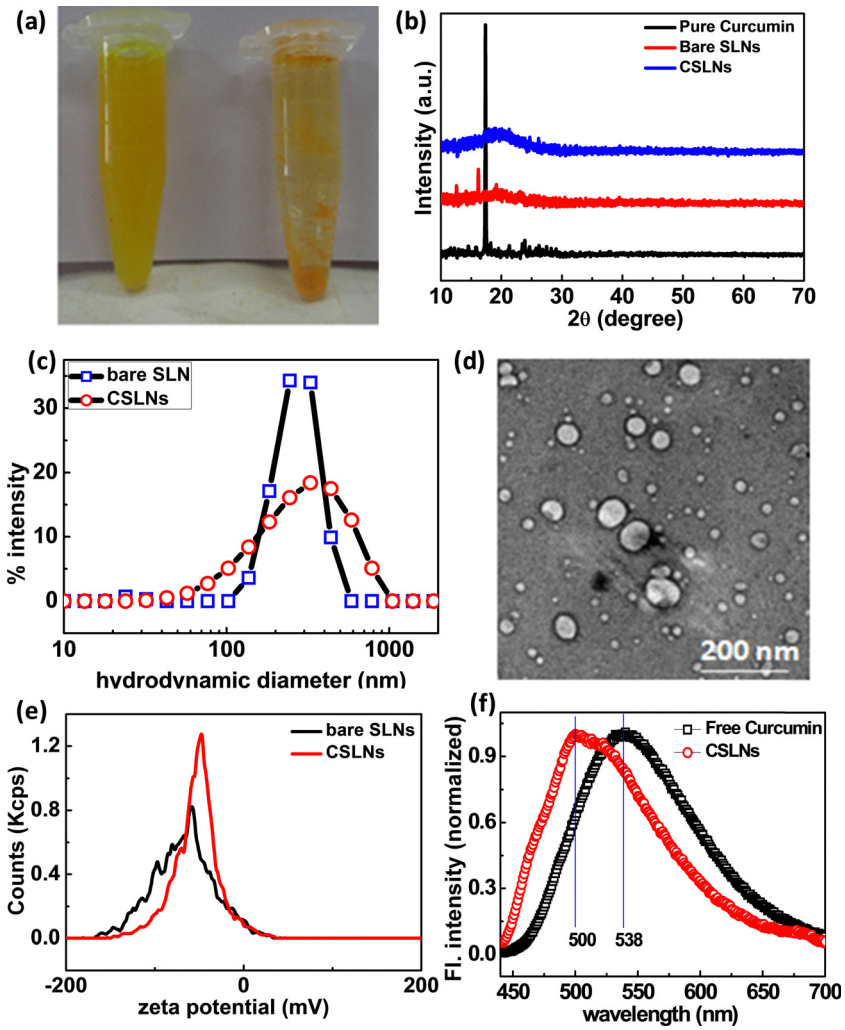

Fig. 1 (a) Curcumin in SLN matrix and water at 30 °C, (b) X-ray diffraction (XRD) patterns of curcumin, bare SLNs and CSLNS, (c) intensity-weighted average hydrodynamic diameter of bare SLN and CSLNs, (d) cryo-transmission electron microscopy (TEM) image of curcumin-loaded solid lipid nanoparticles (CSLNs), scale bar, 200 nm, (e) zeta potential value of bare SLN and CSLNs and (f) normalized fluorescence emission spectra of pure curcumin in methanol and curcumin-loaded SLNs (CSLNs) in water.

it in submicron lipid particles. After forming a suspension of equal amounts of free CUR and CSLNs in an equal volume of PBS solution of pH 7.4, it was observed that the CSLNs formed a stable and homogenous dispersed system, but a significant amount of insoluble curcumin crystals was observed in the curcumin–water mixture, indicating the significant improvement in the dispersibility of curcumin in the water medium after encapsulation in the lipidic structure (Fig. 1(a)). The diffraction pattern in Fig. 1(b) shows the disappearance of sharp crystalline peaks of curcumin in the curcumin-loaded SLNs. This confirms the entrapment of the amorphous curcumin inside the lipid matrix. The similar patterns of both the bare SLNs and CSLNs further suggest that curcumin encapsulation had no effect on the physical structure of the nanoparticles. To evaluate the morphology of the CSLNs, cryo TEM was carried out, which indicated the formation of roughly spherical and smooth solid lipid nanoparticles with a size in the range of 70–100 nm (Fig. 1(d)).[42]

The average hydrodynamic diameter of the colloidal dispersion of CSLNs was measured using the dynamic light scattering technique, as shown in Fig. 1(c). The intensity-weighted average diameter of the bare SLN and CSLNs was found to be 250 ± 4 and 264 ± 12, with a polydispersity index of 0.20 and 0.28, respectively. This higher relative hydrodynamic diameter in comparison to the size obtained from TEM can be explained in terms of the polydispersity as well as the associated hydrated layer along the nanoparticles. The stability of the CSLNs is largely dependent on their surface features, *i.e.* surface charge to be precise. The average zeta potential value of these prepared CSLNs was about −45.7 ± 0.4 mV, as presented in Fig. 1(e). This large negative zeta potential value makes them highly stable as a colloid in the water dispersion and prevents the agglomeration. The minute difference in surface charge between bare SLNs and CSLNs further confirms that most of the curcumin is encapsulated inside the hydrophobic lipid matrix of the SLNs rather than being adsorbed on the surface. Thus, to further

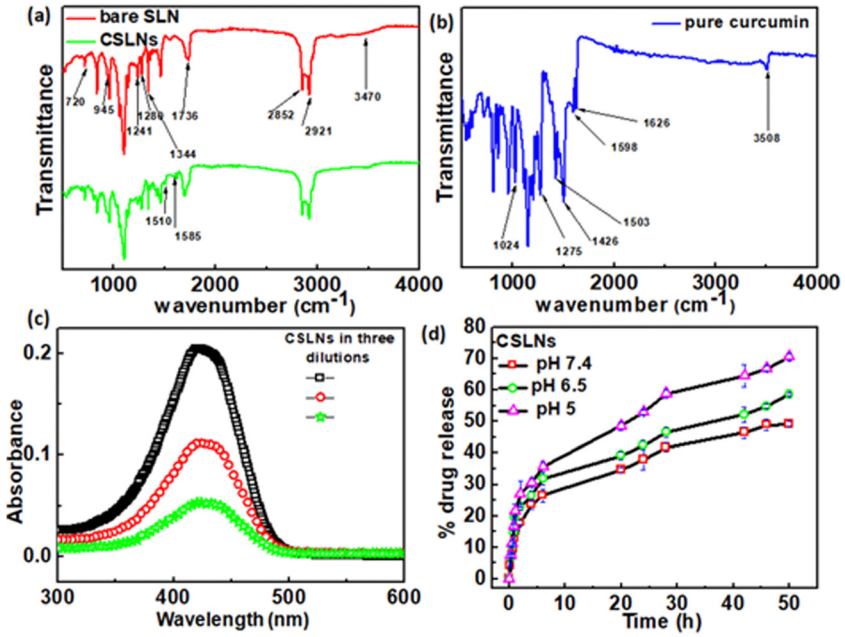

Fig. 2 FTIR spectra of (a) pure curcumin, (b) bare SLN and CSLNs, (c) UV-vis spectra of CSLN dispersion (dilutions were made for ease of calculation) and (d) *in vitro* release profile of curcumin from CSLNs at different pH medium (data are presented as the mean (%) ± std from triplicate measurements).

augment the structural orientation of the curcumin inside the solid lipid matrix, the fluorescence emission spectra of both pure curcumin in methanol and CSLN dispersion were recorded. It was observed that there was shift in the emission maximum from 538 nm to 500 nm from pure curcumin to CSLN sample. There was also an enhancement in the emission observed (here only normalized spectra plotted). The fluorescence of curcumin purely depends on the polarity of its environment, which showed a shift in the emission maximum from a longer to shorter wavelength and increase in fluorescence intensity. This purely indicates the movement of curcumin from a relatively high polar to less polar medium, *i.e.* encapsulation of curcumin happened *via* hydrophobic interaction in the CSLNs (Fig. 1(f)).[43]

To confirm the encapsulation of curcumin in the solid lipid nanoparticles, FTIR measurements were performed. Fig. 2(a) shows the signature peaks of curcumin at 1024 cm^{-1} (C–O–C stretching vibrations), 1275 cm^{-1} (aromatic C–O stretching vibrations), 1426 cm^{-1} (olefinic C–H bending vibrations), 1503 cm^{-1} (C═O and C═C vibrations), 1598 cm^{-1} (benzene ring stretching vibrations), 1626 cm^{-1} (aromatic moiety C═C stretching) and 3508 cm^{-1} (phenolic O–H stretching vibration).[44] Fig. 2(b) shows the peaks corresponding to the bare solid lipid nanoparticles, including the typical peaks of phospholipid at 1241 cm^{-1} (PO_4 antisymmetric stretching bands), 1736 cm^{-1} (symmetrical C═O stretching vibration), 2852 cm^{-1} and 2921 cm^{-1} (CH_2 stretching vibration); lauric acid at 720 cm^{-1} (out-of-plane –C–H bending), 945 cm^{-1} (wagging vibration peak of O–H), 1280 cm^{-1} (stretching vibration of C–O);[45] P188 at 1344 cm^{-1} (–O–H bending), and 3470 cm^{-1} (–O–H stretching). The stretching vibration of $-CH_3$ is masked with the $-CH_2$ stretching vibration at 2924 cm^{-1}.[46] The FTIR spectra of CSLNs showed all the signature peaks of curcumin and bare lipid nanoparticles, as mentioned above. The peak position as well as the shape were similar in CSLNs to that of the phospholipids at 2921 cm^{-1} and 2852 cm^{-1} ($-CH_2$ stretching vibration) and all the related ones.

3.2. Drug loading and release study

The drug encapsulation ability and subsequent drug release pattern of CSLNs were investigated. % EE and % LC are significant parameters in nanoformulations because of their dose rate-related parameters to avoid any unwanted side effects and long-term stability under biological conditions.[47,48] The EE and LC of CSLNs were measured using the centrifugation method, followed by concentration estimation using the UV-Vis method, as mentioned earlier. The drug-loading capacity and encapsulation efficiencies of CSLNs were found to be around 22.8% and 86.5%, respectively (Fig. 2(c)). This high drug loading will help reduce the dose rate and dosage volume. The higher affinity of lipophilic curcumin towards the hydrophobic lipid matrix facilitated a higher and stable curcumin encapsulation in the core.[49] The high drug (curcumin) loading capacity of CSLNs is directly related to lipophilicity of curcumin itself. The reported log P value of curcumin is 3.2. The synthesized SLNs were made up of lipid molecules with long alkyl chains, which cause the curcumin molecules to show even higher affinity towards lipid molecules. This enhanced affinity between the drug and lipid matrix induces extremely stable drug encapsulation in the hydrophobic core. Moreover, the process used here is cold homogenization, which can actually overcome the problems of the hot homogenization technique such as accelerated degradation of the drug at elevated temperature, partitioning and consequent loss of drug molecules

Table 1 Mathematical models for drug release kinetics

Model	Zero order	First order	Higuchi	Hickson–Crowel	Weibull
pH 7.4	0.8626	0.1096	**0.9791**	0.5411	**0.9875**
pH 6.5	0.8575	0.1016	**0.9673**	0.4994	**0.9839**
pH 5	0.8709	0.1044	**0.9759**	0.5257	**0.9866**

into the aqueous phase during the homogenization procedure. Furthermore, the uncertain polymorphic transitions of the lipid at high temperature owing to the complexity of the crystallization step of the nanoemulsion also sometimes lead to the degradation of the host matrix. In the cold homogenization process used in this work, the drug containing melt was rapidly cooled (using ice) to favour a complete and enhanced homogenous drug distribution in the lipid matrix. Thus, by avoiding the aforementioned major drawbacks, the CSLN formulation system could achieve a significantly high drug loading capacity.[50] The pH-dependent drug release profile was monitored for a period of 50 h *via* the dialysis membrane method using reservoir-sink condition to mimic the intracellular condition. The *in vitro* release profile of the CSLNs showed a biphasic release pattern with a burst release of curcumin of 26.5%, 31.8% and 35.5% at pH 7.4, 6.5 and 5, respectively, up to 6 h, followed by slow and sustained release until after 50 h in the medium (Fig. 2(d)). With an increase in the acidity of the medium, the cumulative % release of curcumin was found to increase from 49.3% to 70.5%. The release feature of this curcumin may be due to the distribution of the drug in the CSLNs. In addition, mathematical models including zero-order, first-order, Higuchi, Hixson–Crowell, Korsmeyer–Peppas and Weibull equations were used to further understand the release mechanism of curcumin from CSLNs (Table 1). Model simulation and data analysis were carried out using the KinetDS 2.0 software. Among the equations, the release of curcumin from CSLNs followed the Weibull and Higuchi model the best, given that these two models showed the best fit (R^2 value). According to these two models, curcumin was first dissolved in the solid lipid matrix, and then diffused to the surface of the lipid core, followed by dissolution into the aqueous phase from the matrix.[51–53] Subsequently, the released curcumin from CSLNs diffused from the dialysis bag to the release medium due to the concentration gradient. The diffusion of curcumin was better controlled by encapsulation during the release process. The initial slight burst may be due to the minimal adsorption of curcumin and curcumin located at the peripheral region of CSLNs. Subsequently, the drug incorporated in the core was released in a prolonged period, as shown in Fig. 2(d).[54,55]

3.3 Chemical and storage stability

To determine the chemical stability of the encapsulated curcumin in CSLNs, we carried out time-dependent spectral measurement in both 0.1 M PBS (pH 7.4) and 10% DMEM medium (image, Fig. 3(a)). It was found that the free curcumin almost readily degraded within 15 min of incubation in the vial. In contrast, the CSLN dispersion was found to be highly chemically inert in both media even after 6 h of incubation (Fig. 3(b)). The residual curcumin content in CSLNs remained at 78% and 65% in 10% DMEM and PBS medium, whereas the free curcumin got degraded rapidly by almost 85% and 88% in DMEM and PBS medium after 6 h of incubation, respectively. This result essentially proved that SLN could effectively protect the curcumin from degradation in the solution stage for a longer period. The storage stability for any nanoformulation is

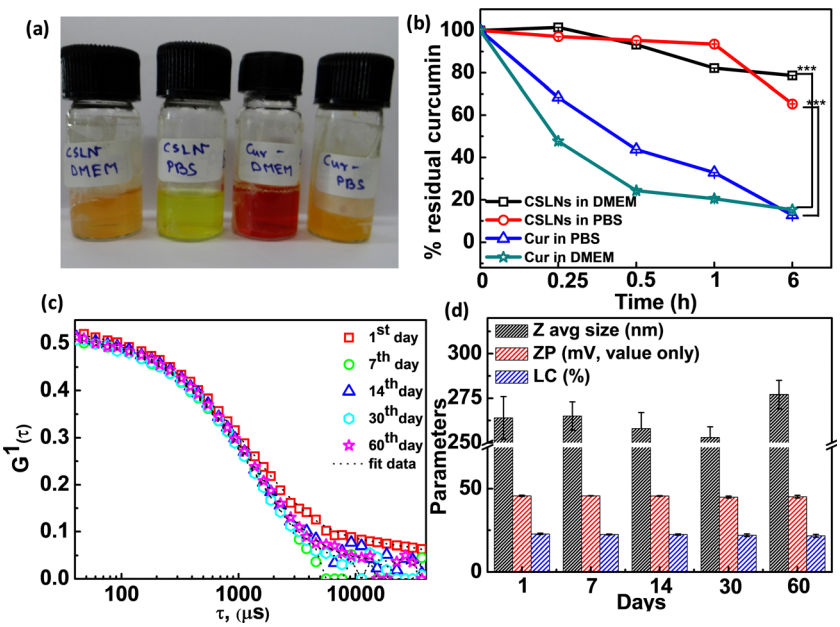

Fig. 3 (a) CSLNs and free curcumin in 10% cell culture (DMEM) and PBS medium, (b) chemical stability of free curcumin and the CSLNs in PBS (pH 7.4) and 10% DMEM medium, (c) comparative autocorrelation functions of CSLNs at different time scales and (d) changes in *Z* average diameter, zeta potential (negative sign not mentioned in graph) and % drug loading content in CSLNs during storage at 4 °C.

Table 2 Data representing the stability parameters (data presented as mean ± SD, n = 3)

S. no.	Avg. hydrodynamic diameter (nm)	Poly dispersity index	Zeta potential (mV)	% LC
1st day	264 ± 12	0.28 ± 0.06	−45.7 ± 0.4	22.8 ± 0.4
7th	265 ± 8	0.27 ± 0.02	−45.7 ± 0.1	22.4 ± 0.3
14th	258 ± 9	0.29 ± 0.04	−45.6 ± 0.2	22.4± 0.4
30th	253 ± 6	0.29 ± 0.01	−44.9 ± 0.6	22.0 ± 0.8
60th day	277 ± 8	0.29 ± 0.04	−45.2 ± 0.8	21.6 ± 0.9

an extremely important parameter for long-term usage with respect to the leakage of the active ingredients and agglomeration.[56] The physical stability of the CSLN system was monitored in terms of average size, surface charge and % loading content. The lyophilized powder of the formulations was stored at 4 °C separately. The mean hydrodynamic diameter changed from 264 ± 6 nm to 277 ± 8 nm only after 60 days of encapsulation (Fig. 3(c)). The surface charge essentially remained almost unchanged at around −45.2 ± 0.8 mV. It was observed that the % drug loading capacity changed from 22.8% to 21.6% after 2 months (Fig. 3(d)). It can be inferred that the curcumin-loaded negatively charged solid lipid nanoparticles were highly stable upon storage at low temperature (which inhibits their thermal degradation) given that no instability was observed even after 60 days storage in powder form, as shown in Table 2.[57]

3.4. *In vitro* studies

3.4.1. CSLN caused alteration in cell morphology and decreased proliferation. The cytotoxic effect of CSLNs at various concentrations (*i.e.* 1–50 μM, 24 and 48 h) in A549 cells was assessed using the MTT assay (Fig. S1, ESI†), which showed IC50 in the range of ∼32 to 12 μM (at 24–48 h). Therefore this concentration range (10–40 μM) was selected for further *in vitro* experiments.

Bright-field microscopy was performed on A549 and WI26 cells treated with increasing concentrations of CSLN (10–40 μM), CUR (10–40 μM) and bare NP (SLN, 100 μg mL^{-1}) for 24–48 h. Representative images of indicated treatments are shown in Fig. 4(a), which show the concentration-dependent effect of CSLN on the morphology alterations in the A549 cells. CSLN caused significantly higher cell death (observed as small, detached and rounded cellular bodies) compared to CUR at equivalent concentrations (10 and 20 μM). It is evident that CSLNs at 40 μM induced significantly higher dead cells (rounded off) with an apoptotic morphology compared to the respective CUR treatment. Bare NP treatment (SLN, 100 μg mL^{-1}) caused no visible morphological alteration compared to the control in both the A549 and WI26 cells. Representative images of the indicated treatments on WI26 cells are depicted in Fig. 4(b), which showed that both CSLNs as well as CUR caused significantly less cytotoxicity to WI26 normal lung cells than the A549 lung cancer cells.

To further study the effect of CSLN on the proliferation of lung cancer cells in comparison to normal lung cells, the MTT

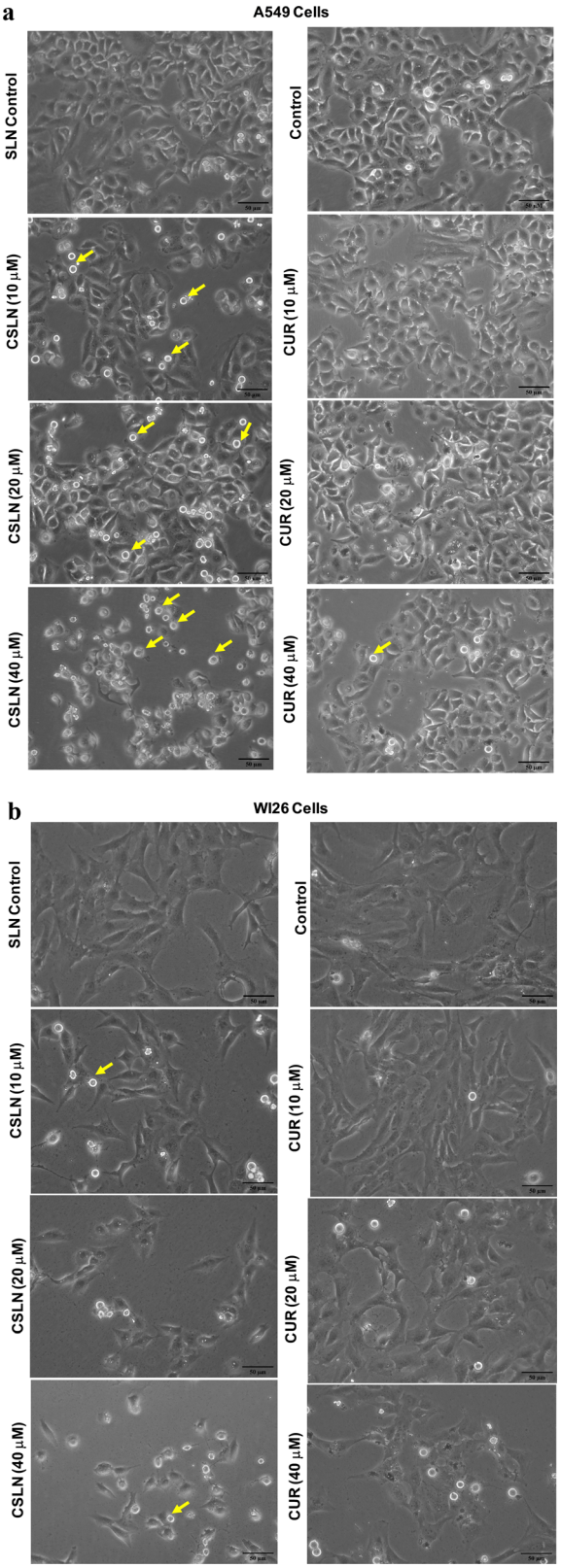

Fig. 4 (a) Phase contrast microscopy images of control, CSLN (10–40 μM), CUR (10–40 μM) and bare NP (SLN, 100 μg mL^{-1})-treated A549 cell line after 24 h of indicated treatment. Scale bar represents 50 μm. Yellow arrows mark the dead cells. (b) Representative phase contrast microscopy images of control, CSLN (10–40 μM), CUR (10–40 μM) and bare NP (SLN, 100 μg mL^{-1})-treated WI26 cell line after 24 h of indicated treatment. Scale bar represents 50 μm. Yellow arrows are mark the dead cells.

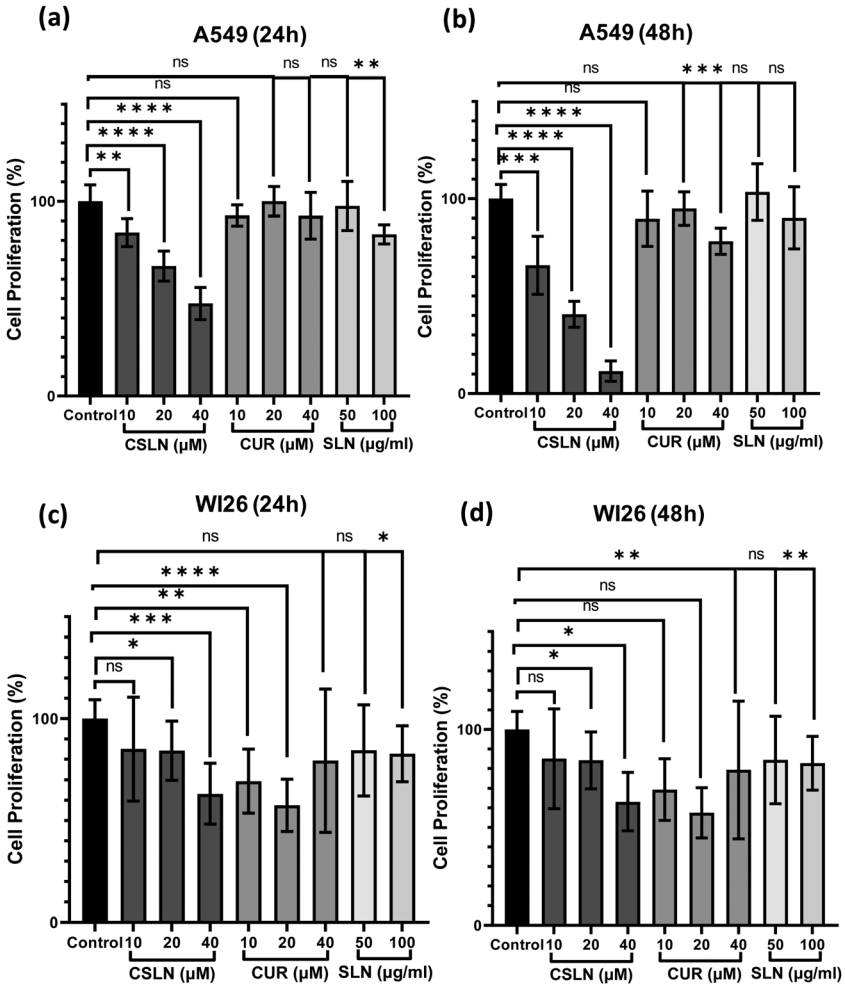

Fig. 5 Percentage proliferation of A549 cells after 24 h (a) and 48 h (b) of treatment with CSLN (10–40 μM), CUR (10–40 μM) and SLN (bare NP, 100 μg mL^{-1}). Percentage proliferation of WI26 cells after 24 h (c) and 48 h (d) of treatment with CSLN (10–40 μM), CUR (10–40 μM) and SLN (bare NP, 100 μg mL^{-1}).

assay was performed. The results showed that a CSLN dose as low as 10 μM significantly decreased the proliferation of lung cancer cells (A549), which followed a concentration- and time-dependent pattern (Fig. 5(a) and (b), respectively). However, the

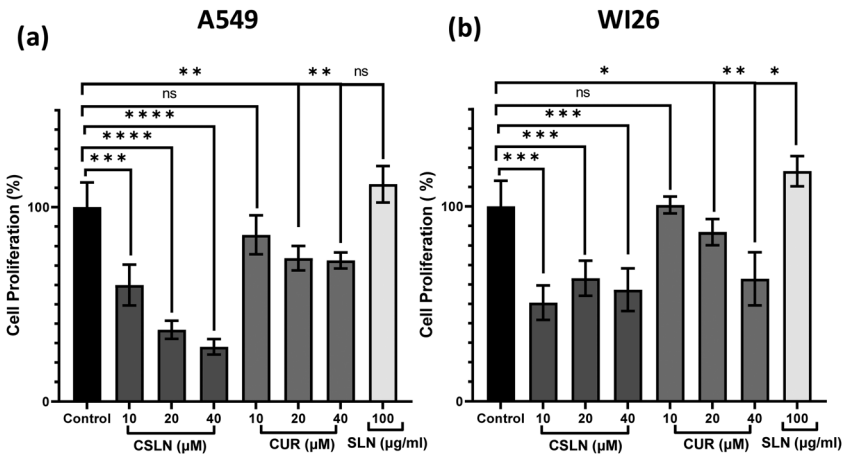

Fig. 6 Effect of indicated treatments on the growth of A549 (a) and WI26 (b) cells assessed by cell count analysis. The values are mean ± SD for three independent experiments performed in triplicate. *$p < 0.05$, **$p < 0.01$, ***$p < 0.001$, and ****$p < 0.0001$ compared to the control group.

unformulated form of CUR (10 and 20 μM) did not significantly affect the proliferation (or mitochondrial metabolic activity) of the cancer cells even up to 48 h. At 40 μM, CUR was found to cause ~20% decrease in cell proliferation after 48 h. Notably, the bare NP, *i.e.* SLN, did not cause any significant decrease in proliferation up to 100 μg mL^{-1}. These results suggest that the SLN form of CUR exerted its cytotoxic activity. Thus, it was imperative to also determine the effect of CSLN on the growth of normal human lung epithelial cells (WI26). The results clearly showed that the effect of CSLN on the growth of WI26 normal cells was found to be less than that on cancerous cells (A549) (Fig. 5(c) and (d), respectively), suggesting a therapeutic window for CSLNs as an anticancer drug. In this case, to further validate the effect of CSLN on cell proliferation, the cell count was measured after 24 h and 48 h of indicated treatments (Fig. 6(a) and (b), respectively). The results showed that CSLN has significantly decreased cell proliferation, which was found to be higher than the effect of native CUR and bare NPs at both 24 and 48 h.

3.4.2. Cellular internalization. To study the cellular internalization of CSLNs in comparison to CUR, immunofluorescence analysis was performed on both A549 and WI26 cells. The results showed that the fluorescence intensity associated with CSLN (10–40 μM) significantly increased (by 2.0–4.5 fold) in the A549 cells treated with CSLNs (Fig. 7(a) and 8(a)) compared to the vehicle control, suggesting the internalization of the CSLN particles in the cancer cells. The curcumin-associated fluorescence was significantly higher in the CSLN-treated cells than in the CUR-treated cells at 40 μM, suggesting the increased uptake of curcumin mediated by CSLN than by pure CUR. The differential uptake of curcumin further explained the higher cancer cell cytotoxicity of CSLN than CUR (Fig. 4–6).

In the WI26 cells, the curcumin fluorescence in the CSLN-treated cells was found to be similar to that in the CUR-treated cells (Fig. 7(b) and 8(b), respectively). These results suggest that the normal lung cells were refractory to take up CSLN or unformulated curcumin. This seemed to be associated with the lesser toxicity of CSLN and CUR to normal cells (WI26) compared to cancer cells (A549), as observed in previous results (Fig. 4–6). These results suggest the potential of CSLNs for application as an anticancer drug.

Interestingly, the curcumin fluorescence in the CSLN-treated A549 cells was found to be mainly localized in their nucleus (Fig. 7(a)). In contrast, the A549 cells treated with free curcumin showed fluorescence localization mostly in their cytoplasm (Fig. 7(a)). The analysis using the NIH Image-J application revealed ~2–4-times higher accumulation of curcumin in the nucleus of the A549 cells treated with CSLNs compared to the WI26 cells treated with CSLNs at the respective concentration (Fig. 8(c) and (d)), respectively. This differential accumulation of curcumin in the nucleus of the cancer cells (in comparison to normal cells) by CSLNs indicated their possible mechanism of anticancer activity in their nucleus as a DNA binding/damaging agent, which was reported previously in cell-free DNA interaction studies with curcumin.[58] Moreover, previous reports showed that smaller Cur-NPs (~28 nm) were

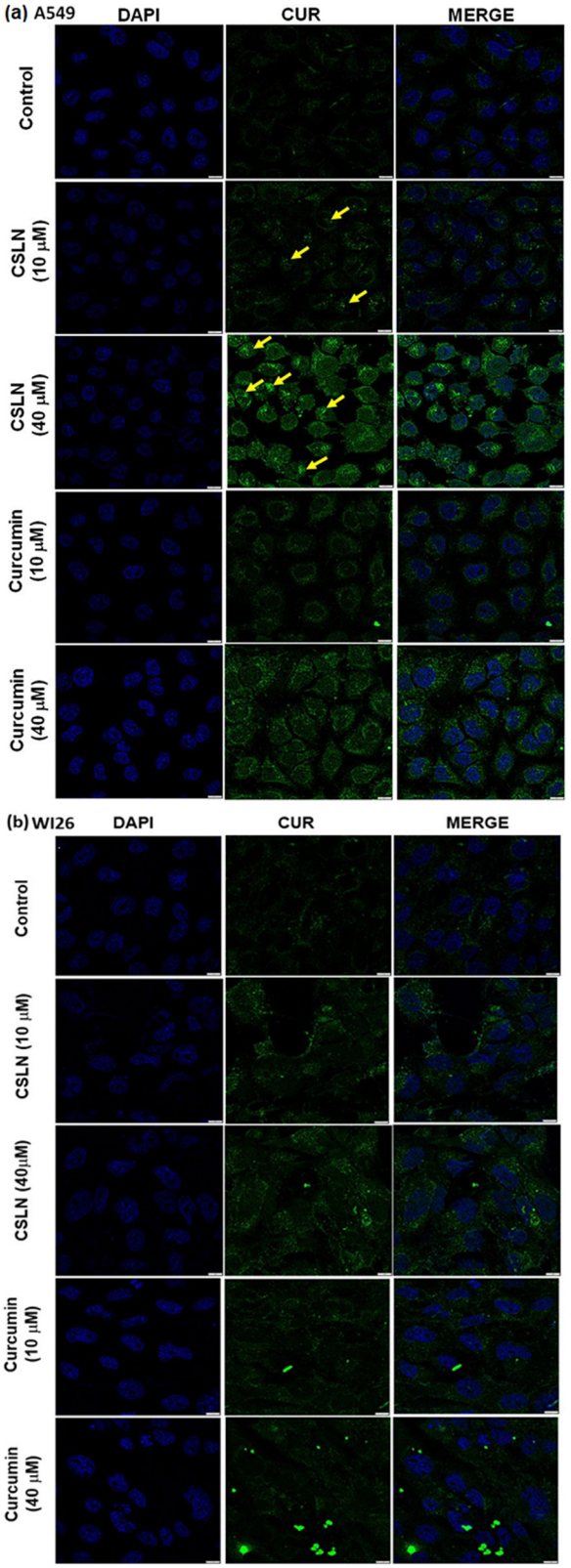

Fig. 7 (a) Representative immunofluorescence images of indicated treatments in A549 cells. Green fluorescence indicates the uptake of curcumin by cells treated with different concentrations of CSLN or CUR. Nuclei were stained with DAPI (blue). Scale bar represents 10 μm. (b) Representative immunofluorescence images of indicated treatments on WI26 cells. Green fluorescence indicates the uptake of curcumin by cells treated with different concentrations of CSLNs or CUR. Nuclei were stained with DAPI (blue). Scale bar represents 10 μm.

internalized more efficiently in the nucleus of cancer cells and caused higher cytotoxicity than larger Cur-NPs (~100–200 nm).[59–61] In the present study, CSLNs (hydrodynamic diameter of ~250 nm) in comparison to bare SLNs were found to localize more significantly inside the nucleus of A549 cells compared to normal human lung epithelial cells (WI26) (Fig. 8(a)–(d)), suggesting the plausible role of physicochemical properties including surface coating of CSLNs as well as cancer cell-specific mechanisms (macropinocytosis) for the internalization of the nanoparticles and their intracellular localization. The high zeta potential of CSLNs (−45.7 ± 0.4 mV) in the present study indicated their greater resistance/stability against agglomeration due to the repulsion between the similarly charged nanoparticles. NPs with high zeta potential (−25 to −55 mV) were found to show a significant correlation with cellular uptake in both non-phagocytic (A549) and phagocytic cells.[62] Other factors such as hydrodynamic size, shape and agglomeration status have also been reported to influence the cellular uptake of NPs.[63] However, no significant correlation was observed between hydrodynamic size and cellular uptake by A549 cells of identical polystyrene nanoparticles conjugated with different functional groups.[62] Therefore, in the present study, the high zeta potential of CSLNs (~250 nm) may possibly play a key role in their cellular internalization.

3.4.3. CSLN-induced apoptosis: sub-G1 FACS analysis. To reveal the cell death-inducing ability of CSLNs, an experiment was performed to quantify the cells in the sub-G1 peak after propidium iodide staining using FACS analysis. The results showed that CSLNs (10 and 40 μM) significantly ($p < 0.0001$) increased the relative fold change (5–13 fold) of cells (9–18%) in the sub-G1 phase compared to the control cells (~1.5%) and cells treated with an equimolar concentration of CUR in A549 cells (Fig. 9(a)). Consistent with the above-mentioned results (Fig. 5 and 6), CSLNs were also found to be less toxic to the WI26 normal human lung cells in terms of cell death by sub-G1 analysis. The results showed that CSLN (10 and 40 μM) less significantly ($p < 0.01$) increased the relative fold change (1.1–1.5 fold) of cells (7–10%) in the sub-G1 phase compared to the control cells (~6.5%) and cells treated with an equimolar concentration of CUR in WI26 cells (Fig. 9(b)). Given that the

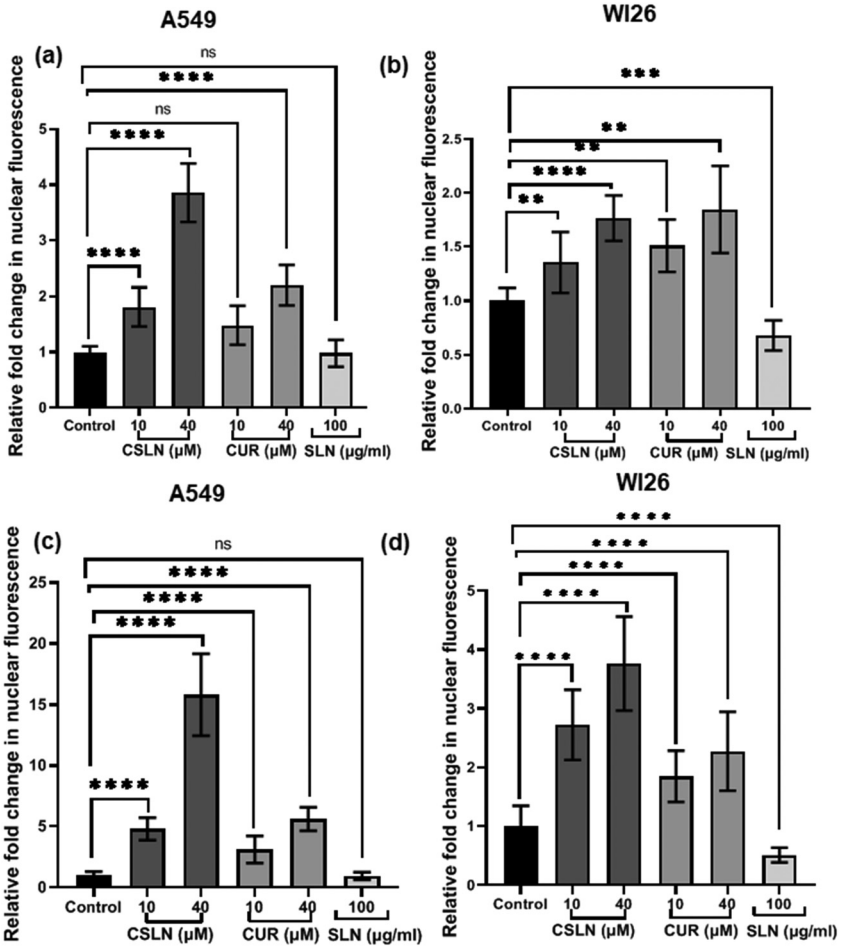

Fig. 8 Relative fold change in mean fluorescence intensity of curcumin in various treatment groups in A549 cells (a) and WI26 cells (b). Data represents mean of fluorescence normalized with DAPI fluorescence from randomly selected images (10 to 15). Nuclear localisation of curcumin by CSLN in A549 cells (c) and WI26 cells (d) compared to CUR and SLN alone. Data represents mean of nuclear fluorescence from randomly selected cells (80 to 100 cells).*$p < 0.05$, **$p < 0.01$, ***$p < 0.001$, and ****$p < 0.0001$ compared to respective control group or indicated comparison.

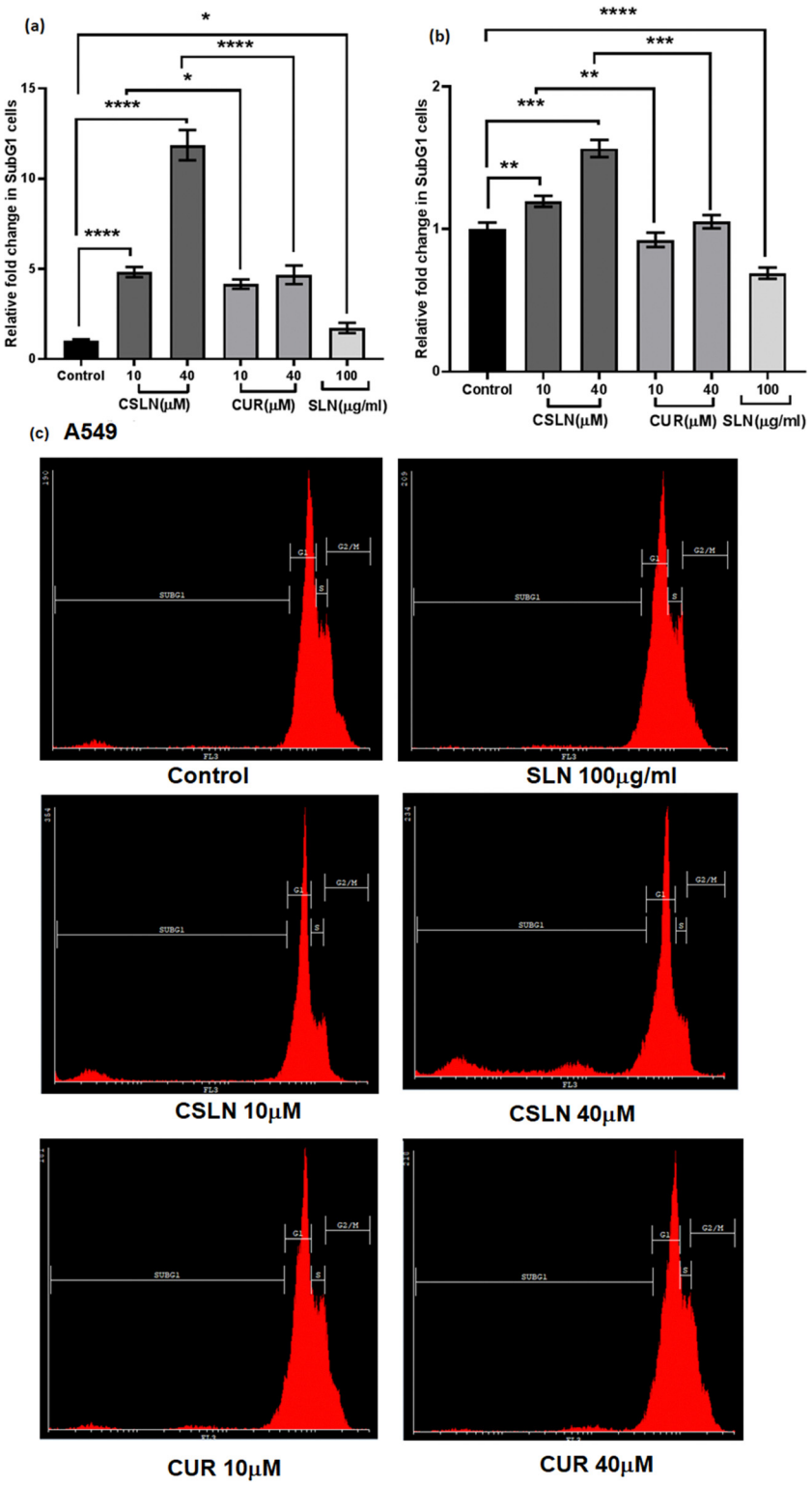

Fig. 9 Cell death analysis by sub-G1 peak of cell cycle distribution after PI staining using flow cytometry of control or CSLN/CUR-treated A549 cells (a) and WI26 cells (b). Cells were treated with the specified concentration of CSLN or CUR (10 and 40 μM) and SLN (bare NP, 100 μg mL^{-1}) for 24 h. Relative fold change of cells in sub-G1 phase of cell cycle ± SD compared to control was determined from three independent treatments. (c) Representative histogram showing the distribution of cells in sub-diploid (G1) phase of cell cycle at 24 h under different treatment conditions. *$p < 0.05$, **$p < 0.01$, ***$p < 0.001$, and ****$p < 0.0001$ compared to respective control group or indicated comparison.

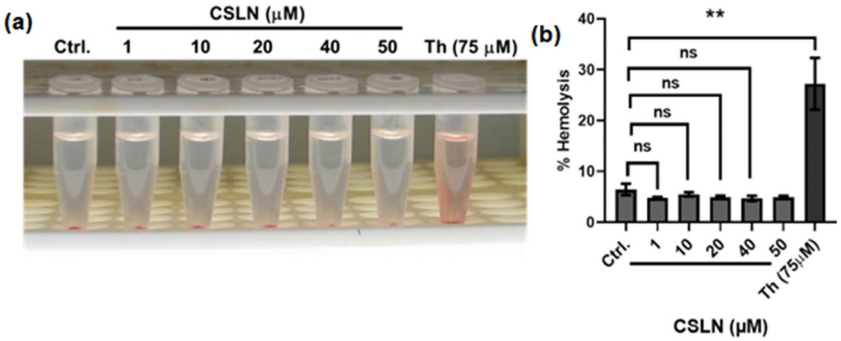

Fig. 10 Effect of CSLNs on human erythrocytes using *ex vivo* hemolysis assay. (a) Image showing clear supernatant in the representative tubes of CSLN-treatment at indicated concentrations compared to control. Thorium metal (75 μM) taken as a positive control to induce hemolysis showed significant leakage of haemoglobin in the supernatant. (b) Hemolysis was measured by measuring the absorbance of the supernatant at 540 nm using spectrophotometer. Data represents mean ± SD derived from three independent treatments. $^{**}p < 0.01$, ns: not significant compared to control.

sub-G1 peak represents cells with nuclear condensation, a characteristic marker of apoptosis, these results provide evidence for the apoptotic mode of cell death induced by the CSLN formulation.

3.5. Erythrocyte toxicity

To explore the *in vivo* potential of CSLNs, their toxicity to erythrocytes was examined using a hemolysis assay. The results showed that a concentration of CSLNs from 1 to 50 μM did not cause any significant increase in hemolysis compared to the control (Fig. 10(a) and (b)), respectively. Thorium, which has been reported to be haemolytic, was employed as a positive control in the experiment.[36] The representative tubes of CSLN-treated erythrocyte suspension showed a clear supernatant or negligible leakage of haemoglobin from the erythrocytes as in the untreated control tube. In contrast, the thorium-treated tube (75 μM) exhibited significant leakage of haemoglobin in the supernatant. These results suggest the biocompatibility of CSLNs for further their preclinical/clinical evaluation.

3.6. *In vivo* studies

Sub-acute toxicity studies provide a discrete hint about any sort of adverse effect of the test formulation, which is stimulated by regular exposure and its cumulative effect on tissue and other important parameters. This is helpful for calculating the appropriate concentration for dosage and the effect of the formulation on individual organs.[64] The sub-acute study was conducted for 4 weeks (28 days) with three different groups, *i.e.*, control (no treatment), bare SLNs (only nanocarrier), and CSLNSs (formulation @200 mg kg^{-1} day^{-1}). The estimated parameters were body weight, haematological, blood biochemistry and histopathological parameters.

3.6.1. Body weight measurement. One of the most important parameters for toxicology investigation is body weight monitoring because an abnormal gain or loss in weight is a direct signature of an immunotoxic effect on the body. Fig. 11(b) shows the relative change in the body weight profile for the three groups. The body weight recorded at 7-day intervals showed a steady transition with respect to weight gain during the study period. Thus, we can infer that the prepared nanoformulation did not cause any obvious adverse effect due to the absence of a statistically significant difference w.r.t. the control group. During the entire study period, no abnormal

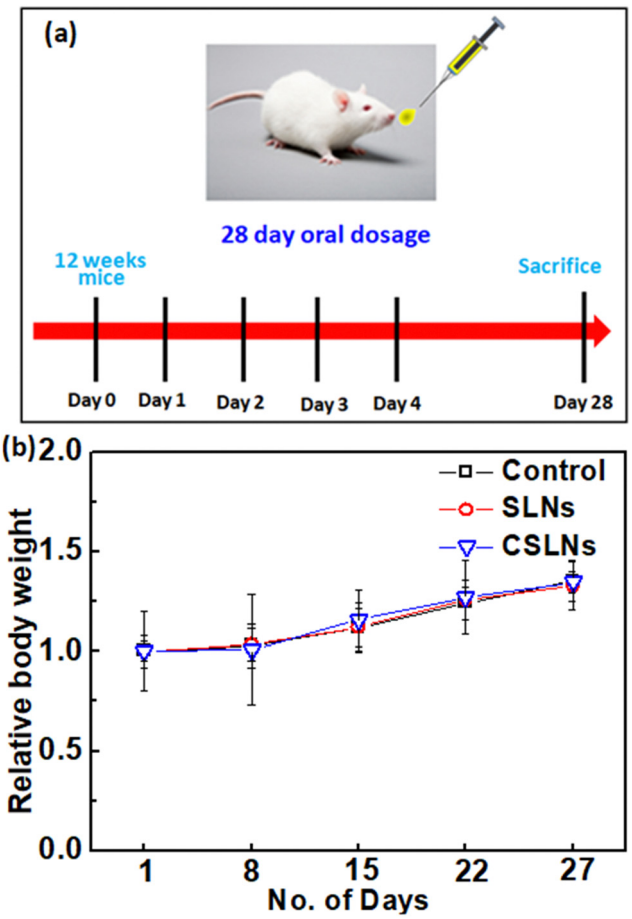

Fig. 11 (a) Scheme of 28 days sub-acute *in vivo* study and (b) average body weight transitions of mice over the 28-day treatment period, where no statistically significant differences in body weight were observed between the treated mice and the non-treated mice. The data are represented as mean ± SEM.

clinical or behavioural changes were detected. Moreover, the necropsy at the end also did not show any macroscopic changes in the organs of the three treatment groups.

3.6.2. Effects on haematological parameters and histopathological examination. Haematological analysis is one of the extremely delicate targets for any new formulation of toxic drugs and chemicals, serving as a significant guide of pathological and physiological effects in animals and humans.[65] The assessment of the haematological parameters could be meaningful in defining the lethal effects of CSLNs on test animal blood, and therefore can be used to explain the blood-related function of CSLNs.[66] In this study, the effect of the formulation on the hematological parameters was observed in different blood parameters. The results showed normal levels of total and differential white blood cells, RBCs, haemoglobin, and packed cell volume compared to the untreated control mice. No sign of thrombocytopenia, leukopenia, anaemia, *i.e.* pancytopenia, was seen in the treated mice (Fig. 12(a) and (b)).

To further augment the confirmation of non-toxicity of the prepared formulation, several biochemical parameters for assessing the liver, kidney and heart functions were monitored. Serum markers such as aspartate transaminase (AST), alanine aminotransferase (ALT) and alkaline phosphatase (ALP) mainly exist in liver cells and their abnormal high concentration in blood is a direct consequence of damage to liver cells, necrosis and hepatotoxicity. The current study revealed no significant difference in the AST, ALT, and ALP levels among the three groups under consideration (Fig. 12(c)). Proteins are the building blocks of living cells. Thus, a change in the level of proteins in the body provides a signal against any type of organ or tissue damage.[67–69] The results here showed no change in the total serum proteins, albumin, and globulin, which implies the absence any liver- and kidney-related malfunctions (Fig. 12(d)). Blood urea nitrogen (BUN), creatinine (CRE) and serum bilirubin are important indicators of kidney function. BUN is a cellular metabolic product and CRE is a particular result of muscle breakdown.

Alternatively, an enhanced level of BUN suggests acute renal dysfunction and a high level of CRE indicates chronic renal dysfunction.[70–72] In the CSLN treatment group, we did not observe any significant difference in the levels of BUN and CRE, demonstrating the non-toxicity effects to the kidneys (Fig. 12(e)). It was also observed that oral administration of CSLNs at the dose rate of 200 mg kg^{-1} per^{-1} day failed to cause any significant change ($p > 0.05$) in the total cholesterol and triglyceride levels of the treated mice compared to the non-treated control group. The random blood sugar, serum phosphorus and calcium levels were also found to be within the

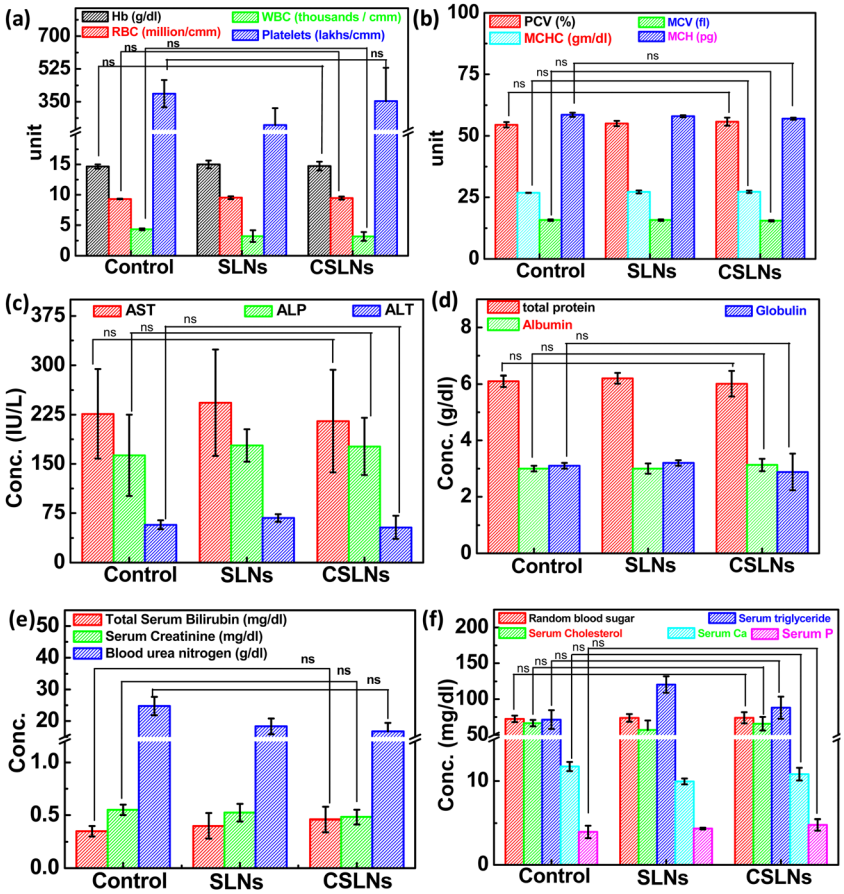

Fig. 12 Effect on blood parameters, serum biochemistry parameters of control mice, blank SLNs and formulation: CSLNs in Swiss albino mouse model and ns: not significant compared to control.

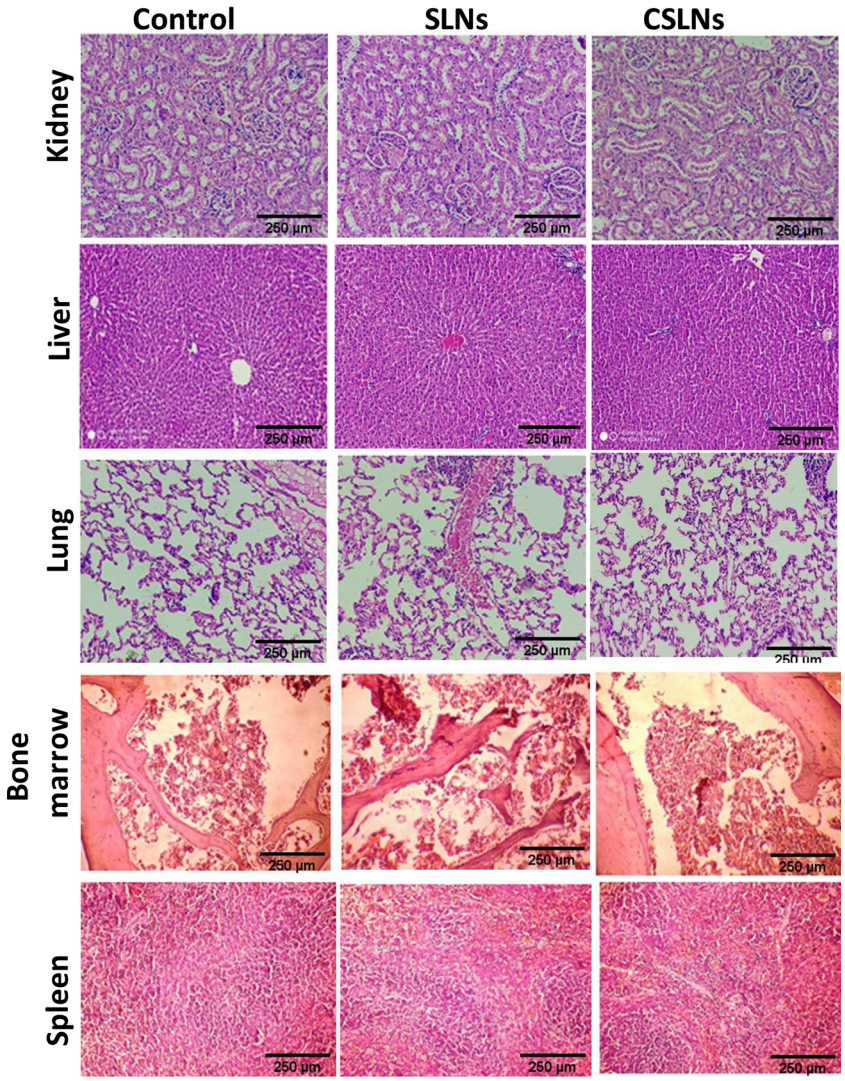

Fig. 13 H&E staining images after 28-day treatment with the control, carrier (SLNs) and formulation (CSLNs). Representative images of kidney, liver, lung, bone marrow and spleen.

range of the control group, suggesting no adverse effect of the formulation on these parameters (Fig. 12(f)).

3.6.3. Histopathological examination. Histopathological evaluation was done on five major organs, namely the kidney, liver, lung, bone marrow and spleen for 28-day study for the control, bare SLNs and CSLNs (formulation). Fig. 13 shows the H&E stained images for the 28-day treatment regimen. All the evaluated organs were found to be completely normal after the treatment with CSLNs for 28 days. The H&E staining of the kidney did not show any adverse effect on the symmetry and overall cellularity of the glomerulus as well as on the thickness of the capillary walls. Pigment accumulation, fatty change, and proliferation of sinusoidal lining cells are some main consequences of toxicity on liver cells. The histopathological assessment by staining showed no hepatocyte degeneration and pigment deposition.[73,74] The two treatment groups showed a normal lung architecture. No substantial change such as increased alveolar cell wall and inflammatory cells were observed in the lung tissue of the treated mice. The H&E images of the bone marrow indicated that there was no significant difference in the cellularity among the different treatment groups. The images showed a normal red pulp area with no cell breakage in the splenic parenchyma.[75–77]

4. Conclusion

We developed a PEGylated solid lipid particle formulation *via* the self-assembly of block copolymers in a lipid emulsion, followed by solvent evaporation. The evaporation-induced freezing of the lipids created submicron particles with a hydrophobic lipid core and hydrophilic PEG shell, which were produced with a narrow polydispersity and specifically targeted lung cancer cells. The lipidic core had the ability to incorporate hydrophobic drugs such as curcumin to an exceptionally high loading capacity of about 23%. This could significantly reduce

the amount of inactive excipients employed in the delivery system, and hence reduce the toxicity of the excipient. Commonly, nanoparticulate delivery systems are susceptible to agglomeration, leading to adverse effects on their pharmacological properties. Alternatively, the present delivery system could be lyophilized and reconstituted using PBS to obtain nanoparticles with a similar size distribution, indicating its stability towards long-term storage. The unusual stability of the particles and their easy dispersibility were attributed to the PEG shell on their surface, which could be easily solvated and remain as a corona to prevent agglomeration. These properties are highly conducive for the development of pharmaceutical formulations. Significant preferential alterations in cell morphology were observed upon the treatment of lung cancer cells with CSLNs. However, bare nanoparticles (without any curcumin) caused no visible morphological alteration compared to the control in both A549 and WI26 cells. More importantly, the PEGylated particles were found to accumulate in the nucleus of the cancer cells compared to the cytoplasm in the normal cells. This could significantly enhance the differential toxicity of the curcumin to lung cancer cells, making it an effective agent for lung cancer therapy. Flow cytometric analysis showed that the treatment of lung cancer cells with CSLNs induced a large increase in the sub G1 phase of the population, compared to that in the normal cells. Given that the sub-G1 peak represents cells with nuclear condensation, a characteristic marker of apoptosis, it indicated the apoptotic mode of cell death induced by the CSLN formulation. The acute oral toxicity evaluation of the formulation in Swiss albino mice indicated that there were no adverse health effects with respect to the drug up to a dose of 200 mg kg^{-1} day^{-1} for 28 days. No signs of thrombocytopenia, leukopenia and anaemia were seen in the treated mice. The histopathological assessment of the major organs such as the kidney, liver, lung, bone marrow and spleen after 28-day exposure showed no hepatocyte degeneration and pigment deposition. These toxicological studies proved the oral safety of the formulation for prolonged administration. Overall, the present formulation has great potential for application in lung cancer management by oral delivery.

Conflicts of interest

The authors declare no competing financial interest.

Acknowledgements

The authors acknowledge Dr A. K. Tyagi, Former Director, Chemistry Group, Bhabha Atomic Research Centre (BARC), India for his constant support and encouragement.

References

1 L. A. Torre, F. Bray, R. L. Siegel, J. Ferlay, J. Lortet-Tieulent and A. Jemal, Global Cancer Statistics, 2012, *Ca-Cancer J. Clin.*, 2015, **65**(2), 87–108.
2 H. Sung, J. Ferlay, R. L. Siegel, M. Laversanne, I. Soerjomataram, A. Jemal and F. Bray, Global Cancer Statistics 2020: GLOBOCAN Estimates of Incidence and Mortality Worldwide for 36 Cancers in 185 Countries, *Ca-Cancer J. Clin.*, 2021, **71**, 209–249.
3 R. A. Ward, S. Fawell, N. Floc'h, V. Flemington, D. McKerrecher and P. D. Smith, Challenges and Opportunities in Cancer Drug Resistance, *Chem. Rev.*, 2020, **121**, 3297–3351.
4 M. E. Deffebach, N. B. Charan, S. Lakshminarayan and J. Butler, The Bronchial Circulation. Small, but a Vital Attribute of the Lung, *Am. Rev. Respir. Dis.*, 1987, **135**, 463–481.
5 L. Eldridge, A. Moldobaeva, Q. Zhong, J. Jenkins, M. R. Snyder, R. H. Brown, W. Mitzner and E. M. Wagner, Bronchial Artery Angiogenesis Drives Lung Tumor Growth, *Cancer Res.*, 2016, **76**, 5962–5969.
6 F. A. Shepherd, J. Crowley, P. Van Houtte, P. E. Postmus, D. N. Carney, K. Chansky, Z. Shaikh and P. Goldstraw, The International Association for the Study of Lung Cancer Lung Cancer Staging Project: Proposals Regarding the Clinical Staging of Small Cell Lung Cancer in the Forthcoming (Seventh) Edition of the Tumor, Node, Metastasis Classification for Lung Cancer, *J. Thorac. Oncol.*, 2007, **2**, 1067–1077.
7 M. Riihimäki, M. Riihimäki, A. Hemminki, M. Fallah, H. Thomsen, K. Sundquist, J. Sundquist, J. Sundquist, K. Hemminki and K. Hemminki, Metastatic Sites and Survival in Lung Cancer, *Lung Cancer*, 2014, **86**, 78–84.
8 A. I. Minchinton and I. F. Tannock, Drug Penetration in Solid Tumours, *Nat. Rev. Cancer*, 2006, **6**, 583–592.
9 S. K. Sriraman, B. Aryasomayajula and V. P. Torchilin, V. P. Barriers to Drug Delivery in Solid Tumors, *Tissue Barriers*, 2014, **2**, e29528.
10 A. Clegg, D. A. Scott, M. Sidhu, P. Hewitson and N. Waugh, A Rapid and Systematic Review of the Clinical Effectiveness and Cost-Effectiveness of Paclitaxel, Docetaxel, Gemcitabine and Vinorelbine in Non-Small-Cell Lung Cancer, *Health Technol. Assess.*, 2001, **5**, 1–195.
11 P. M. Anderson, G. Schroeder and K. M. Skubitz, Oral Glutamine Reduces the Duration and Severity of Stomatitis after Cytotoxic Cancer Chemotherapy, *Cancer*, 1998, **83**, 1433–1439.
12 B. Kalyanaraman, J. Joseph, S. Kalivendi, S. Wang, E. Konorev and S. Kotamraju, Doxorubicin-Induced Apoptosis: Implications in Cardiotoxicity, *Mol. Cell. Biochem.*, 2002, **234–235**, 119–124.
13 E. Lee, J. Lee, I.-H. Lee, M. K. Yu, H. Kim, S. Y. Chae and S. Jon, Conjugated Chitosan as a Novel Platform for Oral Delivery of Paclitaxel, *J. Med. Chem.*, 2008, **51**, 6442–6449.
14 M. Borner, W. Scheithauer, C. Twelves, J. Maroun and H. Wilke, Answering Patients' Needs: Oral Alternatives to Intravenous Therapy, *Oncologist*, 2001, **6**, 12–16.
15 V. J. O'Neill and C. Twelves, Oral Cancer Treatment: Developments in Chemotherapy and Beyond, *Br. J. Cancer*, 2002, **87**, 933–937.

16 H. Maeda, H. Nakamura and J. Fang, The EPR Effect for Macromolecular Drug Delivery to Solid Tumors: Improvement of Tumor Uptake, Lowering of Systemic Toxicity, and Distinct Tumor Imaging *In Vivo*, *Adv. Drug Delivery Rev.*, 2013, **65**, 71–79.

17 L. Fu, Y. Zhang, R. A. Farokhzad, B. B. Mendes, J. Cond and J. Shi, 'Passive'nanoparticles for organ-selective systemic delivery: design, mechanism and perspective, *Chem. Soc. Rev.*, 2023, **52**, 7579–7601.

18 B. Dutta, K. C. B. Barick and P. A. Hassan, Recent Advances in Active Targeting of Nanomaterials for Anticancer Drug Delivery, *Adv. Colloid Interface Sci.*, 2021, **296**, 102509.

19 M. Pandey, A. K. Singh and P. C. Pandey, Synthesis and *in vitro* antibacterial behavior of curcumin-conjugated gold nanoparticles, *J. Mater. Chem. B*, 2023, **11**, 3014–3026.

20 H. Li, M. Zhang, J. He, J. Liu, X. Sun and P. Ni, A CD326 monoclonal antibody modified core cross-linked curcumin-polyphosphoester prodrug for targeted delivery and cancer treatment, *J. Mater. Chem. B*, 2023, **11**, 9467–9477.

21 R. Xu, S. Ye, J. Yan, P. Kumar, F. Zhang and X. Zhao, Microfluidic Formulation of Curcumin-Loaded MultiresponsiveGelatin Nanoparticles for Anticancer Therapy, *ACS Biomater. Sci. Eng.*, 2023, **9**(6), 3402–3413.

22 Y. Peng, S. Yu, Z. Wang, P. Huang, W. Wang and J. Xing, Nanogels loading curcumin in situ through microemulsion photopolymerization for enhancement of antitumor effects, *J. Mater. Chem. B*, 2022, **10**, 3293–3302.

23 Y.-J. Wang, M.-H. Pan, A.-L. Cheng, L.-I. Lin, Y. S. Ho, C.-Y. Hsieh and J.-K. Lin, Stability of curcumin in buffer solutions and characterization of its degradation products, *J. Pharm. Biomed. Anal.*, 1997, **15**, 1867–1876.

24 Z. Stanić, Curcumin, a compound from natural sources, a true scientific challenge–a review, *Plant Foods Hum. Nutr.*, 2017, **72**, 1–2.

25 M. S. Alqahtani, A. S. Alqahtani, A. Al-Thabit, M. A. Roni and R. Syed, Novel lignin nanoparticles for oral drug delivery, *J. Mater. Chem. B*, 2019, **7**, 4461–4473.

26 A. Guri, İ. Gülseren and M. Corredig, Utilization of solid lipid nanoparticles for enhanced delivery of curcumin in cocultures of HT29-MTX and Caco-2 cells, *Food Funct.*, 2013, **4**, 1410–1419.

27 M. Amiri, S. Jafari, M. Kurd, H. Mohamadpour, M. Khayati, F. Ghobadinezhad, O. Tavallaei, H. Derakhshankhah, S. S. Malvajerd, S. S. Malvajerd and Z. Izadi, Engineered Solid Lipid Nanoparticles and Nanostructured Lipid Carriers as New Generations of Blood–Brain Barrier Transmitter, *ACS Chem. Neurosci.*, 2021, **12**, 4475–4490.

28 O. Taratula, A. Kuzmov, M. Shah, O. B. Garbuzenko and T. Minko, Nanostructured Lipid Carriers as Multifunctional Nanomedicine Platform for Pulmonary Co-Delivery of Anticancer Drugs and SiRNA, *J. Controlled Release*, 2013, **171**, 349–357.

29 H. Otsuka, Y. Nagasaki and K. Kataoka, PEGylated Nanoparticles for Biological and Pharmaceutical Applications, *Adv. Drug Delivery Rev.*, 2003, **55**, 403–419.

30 D. Hao, Q. Meng, B. Jiang, S. Lu, X. Xiang, Q. Pei, H. Yu, X. Jing and Z. Xie, Hypoxia-Activated PEGylated Paclitaxel Prodrug Nanoparticles for Potentiated Chemotherapy, *ACS Nano*, 2022, **16**, 14693–14702.

31 W. Mehnert, Solid Lipid Nanoparticles Production, Characterization and Applications, *Adv. Drug Delivery Rev.*, 2001, **47**, 165–196.

32 J. Sun, C. Bi, H. M. Chan, S. Sun, Q.-W. Zhang and Y. Zheng, Curcumin-Loaded Solid Lipid Nanoparticles Have Prolonged *in Vitro* Antitumour Activity, Cellular Uptake and Improved *in Vivo* Bioavailability, *Colloids Surf., B*, 2013, **111**, 367–375.

33 K. C. Barick, Ekta, S. L. Gawali, A. Sarkar, A. Kunwar, K. I. Priyadarsini and P. A. Hassan, Pluronic Stabilized Fe_3O_4 Magnetic Nanoparticles for Intracellular Delivery of Curcumin, *RSC Adv.*, 2016, **6**, 98674–98681.

34 S. Huang, J. He, C. Lei, H. Lin, W. Zhang and Q. Zhong, Improved Physicochemical Properties of Curcumin-Loaded Solid Lipid Nanoparticles Stabilized by Sodium Caseinate-Lactose Maillard Conjugate, *J. Agric. Food Chem.*, 2020, **68**, 7072–7081.

35 B. Dutta, A. Nema, N. G. Shetake, J. Gupta, K. C. Barick, K. C. Barick, M. A. Lawande, B. N. Pandey, I. K. Priyadarsini, P. A. Hassan and P. A. Hassan, Glutamic acid-coated Fe_3O_4 nanoparticles for tumor-targeted imaging and therapeutics, *Mater. Sci. Eng., C*, 2020, **112**, 110915.

36 A. Kumar, M. Ali, B. N. Pandey, P. A. Hassan and K. P. Mishra, Role of Membrane Sialic Acid and Glycophorin Protein in Thorium induced Aggregation and Hemolysis of human erythrocytes, *Biochimie*, 2010, **92**, 869–879.

37 R. Ganguly, G. Verma, A. Ingle, S. Kumar, H. D. Sarma, D. Dutta, B. Dutta, A. C. Kunwar, K. R. Ajish, K. C. Bhainsa, P. A. Hassan and V. K. Aswal, Structural, Rheological and Therapeutic Properties of Pluronic F127 Hydrogel and Beeswax Based Lavender Oil Ointment Formulations, *J. Mol. Liq.*, 2022, **365**, 120157.

38 P. V. Turner, T. Brabb, C. Pekow and M. A. Vasbinder, Administration of Substances to Laboratory Animals: Routes of Administration and Factors to Consider, *J. Am. Assoc. Lab. Anim. Sci.*, 2011, **50**, 600–613.

39 M. K. Malik, P. Bhatt, J. Singh, R. D. Kaushik, G. Sharma and V. Kumar, Preclinical Safety Assessment of Chemically Cross-Linked Modified Mandua Starch: Acute and Sub-Acute Oral Toxicity Studies in Swiss Albino Mice, *ACS Omega*, 2022, **7**, 35506–35514.

40 Y. Cao, Y. Xiaoguang, Y. Wu, J. Yi, Y. Wu, C.-L. Yu, Y. Huang, Y. Bao, L. Sun and Y. Li, Dual release of angiostatin and curcumin from biodegradable PLGA microspheres inhibit Lewis lung cancer in a mice model, *RSC Adv.*, 2016, **6**, 111440.

41 C. A. Pennock, D. Murphy, J. Sellers and K. J. Longdon, A Comparison of Autoanalyser Methods for the Estimation of Glucose in Blood, *Clin. Chim. Acta*, 1973, **48**, 193–201.

42 A. K. K. Leung, I. M. Hafez, S. Baoukina, N. M. Belliveau, I. V. Zhigaltsev, E. Afshinmanesh, D. P. Tieleman, C. L. Hansen, M. J. Hope and P. R. Cullis, Lipid Nanoparticles

Containing SiRNA Synthesized by Microfluidic Mixing Exhibit an Electron-Dense Nanostructured Core, *J. Phys. Chem. C*, 2012, **116**, 18440–18450.

43 A. H. Sneharani, J. V. Karakkat, S. A. Singh and A. G. A. Rao, Interaction of Curcumin with β-Lactoglobulin—Stability, Spectroscopic Analysis, and Molecular Modelling of the Complex, *J. Agric. Food Chem.*, 2010, **58**, 11130–11139.

44 P. Khandelwal, A. Alam, A. Choksi, S. Chattopadhyay and P. Poddar, Retention of Anticancer Activity of Curcumin after Conjugation with Fluorescent Gold Quantum Clusters: An *in Vitro* and *in Vivo* Xenograft Study, *ACS Omega*, 2018, **3**, 4776–4785.

45 Y. Chen, Y. Liu, H. Liu and Y. Gao, Preparation of Lauric Acid Modified High-Amylose Cornstarch by a Solvothermal Process and Its Pickering Emulsion, *ACS Food Sci. Technol.*, 2021, **1**, 845–853.

46 L. Peng, F. Cheng, Y. Zheng, Z. Shi and W. He, Multilayer Assembly of Tannic Acid and an Amphiphilic Copolymer Poloxamer 188 on Planar Substrates toward Multifunctional Surfaces with Discrete Microdome-Shaped Features, *Langmuir*, 2018, **34**, 10748–10756.

47 S. Kim, M. J. Stébé, J. L. Blin and A. Pasc, A, pH-controlled delivery of curcumin from a compartmentalized solid lipid nanoparticle@ mesostructured silica matrix, *J. Mater. Chem. B*, 2014, **2**, 7910–7917.

48 J. Wang, H. Wang, H. Xu, J. Li, X. Zhang and X. Zhang, Solid lipid nanoparticles as an effective sodium aescinate delivery system: formulation and anti-inflammatory activity, *RSC Adv.*, 2022, **12**, 6583–6591.

49 S. Patra, J. Dey and A. Chakraborty, Physicochemical Characterization, Stability, and *in Vitro* Evaluation of Curcumin-Loaded Solid Lipid Nanoparticles Prepared Using Biocompatible Synthetic Lipids, *ACS Appl. Bio Mater.*, 2023, **6**, 2785–2794.

50 S. Mukherjee, S. Ray and R. S. Thakur, Solid lipid nanoparticles: a modern formulation approach in drug delivery system, *Indian J. Pharm. Sci.*, 2009, **71**, 349.

51 T. Wang, X. Ma, Y. Lei and Y. Luo, Solid lipid nanoparticles coated with cross-linked polymeric double layer for oral delivery of curcumin, *Colloids Surf., B*, 2016, **148**, 1–11.

52 C. Y. Loo, D. Traini, P. M. Young, T. Parumasivam and W. H. Lee, Pulmonary delivery of curcumin and quercetin nanoparticles for lung cancer–Part 1: Aerosol performance characterization, *J. Drug Delivery Sci. Technol.*, 2023, **86**, 104646.

53 S. Dash, P. N. Murthy, L. Nath and P. Chowdhury, Kinetic modeling on drug release from controlled drug delivery systems, *Acta Pol. Pharm.*, 2010, **67**, 217–223.

54 M. L. Bondì, M. R. Emma, C. Botto, G. Augello, A. Azzolina, F. Di Gaudio, E. F. Craparo, G. Cavallaro, D. Bachvarov and M. Cervello, Biocompatible Lipid Nanoparticles as Carriers to Improve Curcumin Efficacy in Ovarian Cancer Treatment, *J. Agric. Food Chem.*, 2017, **65**, 1342–1352.

55 B. Dutta, K. C. Barick, G. Verma, V. K. Aswal, I. Freilich, D. Danino, B. G. Singh, K. I. Priyadarsini and P. A. Hassan, PEG Coated Vesicles from Mixtures of Pluronic P123 and L-α-Phosphatidylcholine: Structure, Rheology and Curcumin Encapsulation, *Phys. Chem. Chem. Phys.*, 2017, **19**, 26821–26832.

56 W. Zhou, W. Liu, L. Zou, W. Liu, C. Liu, R. Liang and J. Chen, Storage Stability and Skin Permeation of Vitamin c Liposomes Improved by Pectin Coating, *Colloids Surf., B*, 2014, **117**, 330–337.

57 M. Henderson, Y. Eygeris, A. Jozic, M. Herrera and G. Sahay, Leveraging Biological Buffers for Efficient Messenger RNA Delivery *via* Lipid Nanoparticles, *Mol. Pharmaceutics*, 2022, **19**, 4275–4285.

58 S. Nafisi, M. Adelzadeh, Z. Norouzi and M. N. Sarbolouki, Curcumin Binding to DNA and RNA, *DNA Cell Biol.*, 2009, **28**, 201–208.

59 W. H. Lee, M. Bebawy, C. Y. Loo, F. Luk, R. S. Mason and R. Rohanizadeh, Fabrication of curcumin micellar nanoparticles withenhanced anti-cancer activity, *J. Biomed. Nanotechnol.*, 2014, **11**, 1093.

60 W. H. Lee, C. Y. Loo, H.-X. Ong, D. Traini, P. M. Young and R. Rohanizadeh, Synthesis and Characterization of Inhalable Flavonoid Nanoparticle for Lung Cancer Cell Targeting, *J. Biomed. Nanotechnol.*, 2016, **12**, 371–386.

61 W. H. Lee, C. Y. Loo, D. Traini and P. M. Young, Development and evaluation of paclitaxel and curcumin dry powder for inhalation lung cancer treatment, *Pharmaceutics*, 2020, **13**, 9.

62 J. Clavadetscher, D.-K. Lee, S. V. Chankeshwara, S. V. Chankeshwara, M. Bradley and W.-S. Cho, Surface Charge-Dependent Cellular Uptake of Polystyrene Nanoparticles, *Nanomaterials*, 2018, **8**, 1028.

63 C. Kinnear, T. Moore, L. Rodriguez-Lorenzo, B. Rothen-Rutishauser and A. Petri-Fink, Form Follows Function: Nanoparticle Shape and Its Implications for Nanomedicine, *Chem. Rev.*, 2017, **117**, 11476–11521.

64 R. Ganugula, M. Arora, S. Dwivedi, D. S. Chandrashekar, S. Varambally, E. M. Scott and M. N. V. R. Kumar, Systemic Anti-Inflammatory Therapy Aided by Curcumin-Laden Double-Headed Nanoparticles Combined with Injectable Long-Acting Insulin in a Rodent Model of Diabetes Eye Disease, *ACS Nano*, 2023, **17**, 6857–6874.

65 K. C. Nguyen, Y. Zhang, J. Todd, K. Kittle, D. Patry, D. Caldwell, M. Lalande, S. Smith, D. Parks, M. Navarro, A. Massarsky, T. W. Moon, W. G. Willmore and A. F. Tayabali, Biodistribution and Systemic Effects in Mice Following Intravenous Administration of Cadmium Telluride Quantum Dot Nanoparticles, *Chem. Res. Toxicol.*, 2019, **32**, 1491–1503.

66 M. Yakubu, M. Akanji and A. Oladiji, Hematological Evaluation in Male Albino Rats Following Chronic Administration of Aqueous Extract of Fadogia Agrestis Stem, *Pharmacogn. Mag.*, 2007, **3**, 34–38.

67 L. Rao, Q.-F. Meng, L.-L. Bu, B. Cai, Q. Huang, Z.-J. Sun, W.-F. Zhang, A. Li, S. Guo, W. Liu, T.-H. Wang and X.-Z. Zhao, Erythrocyte Membrane-Coated Upconversion Nanoparticles with Minimal Protein Adsorption for Enhanced Tumor Imaging, *ACS Appl. Mater. Interfaces*, 2017, **9**, 2159–2168.

68 B. T. Doumas, W. Ard Watson and H. G. Biggs, Albumin Standards and the Measurement of Serum Albumin with Bromcresol Green, *Clin. Chim. Acta*, 1971, **31**, 87–96.
69 J. Kim, A. Jozic, Y. Lin, Y. Eygeris, E. Bloom, X. Tan, C. J. Acosta, K. D. MacDonald, K. Welsher and G. Sahay, Engineering Lipid Nanoparticles for Enhanced Intracellular Delivery of MRNA through Inhalation, *ACS Nano*, 2022, **16**, 14792–14806.
70 W. G. Miller, G. L. Myers, E. R. Ashwood, A. A. Killeen, E. Wang, L. M. Thienpont and L. Siekmann, Creatinine Measurement: State of the Art in Accuracy and Interlaboratory Harmonization, *Arch. Pathol. Lab. Med.*, 2005, **129**, 297–304.
71 C. Nehate, A. A. Moothedathu Raynold, V. Haridas and V. Koul, Comparative Assessment of Active Targeted Redox Sensitive Polymersomes Based on PPEGMA-S-S-PLA Diblock Copolymer with Marketed Nanoformulation, *Biomacromolecules*, 2018, **19**, 2549–2566.
72 M. H. Rosner and W. K. Bolton, Renal Function Testing, *Am. J. Kidney Dis.*, 2006, **47**, 174–183.
73 A. Thakkar, S. Chenreddy, A. Thio, W. Khamas, J. Wang and S. Prabhu, Preclinical Systemic Toxicity Evaluation of Chitosan-Solid–Lipid Nanoparticle-Encapsulated Aspirin and Curcumin in Combination with Free Sulforaphane in BALB/c Mice, *Int. J. Nanomed.*, 2016, **11**, 3265–3276.
74 A. Ali, S. Saeed, R. Hussain, G. Afzal, A. B. Siddique, G. Parveen, M. Hasan and G. Caprioli, Synthesis and Characterization of Silica, Silver-Silica, and Zinc Oxide-Silica Nanoparticles for Evaluation of Blood Biochemistry, Oxidative Stress, and Hepatotoxicity in Albino Rats, *ACS Omega*, 2023, **8**, 20900–20911.
75 L. Nie, P. Huang, W. Li, W. Li, X. Yan, A. J. Jin, Z. Wang, Y. Tang, S. Wang, X. Zhang, G. Niu and X. Chen, Early-Stage Imaging of Nanocarrier-Enhanced Chemotherapy Response in Living Subjects by Scalable Photoacoustic Microscopy, *ACS Nano*, 2014, **8**, 12141–12150.
76 M. Nazief, P. S. Hassaan, H. Khalifa, M. Sokar and A. H. El-Kamel, Lipid-Based Gliclazide Nanoparticles for Treatment of Diabetes: Formulation, Pharmacokinetics, Pharmacodynamics and Subacute Toxicity Study, *Int. J. Nanomed.*, 2020, **15**, 1129–1148.
77 J. Liu, F. Erogbogbo, F. Erogbogbo, K.-T. Yong, L. Ye, J. Liu, R. Hu, H. Chen, Y. Hu, Y. Yang, J. Yang, I. Roy, N. Karker, M. T. Swihart and P. N. Prasad, Assessing Clinical Prospects of Silicon Quantum Dots: Studies in Mice and Monkeys, *ACS Nano*, 2013, **7**, 7303–7310.